Causal, Stochastic MPC for Wave Energy Converters

Connor H. Ligeikis and Jeffrey T. Scruggs

***Abstract*— We implement a causal model predictive control (MPC) strategy to maximize power generation from a wave energy converter (WEC) system, for which the power take-off (PTO) systems have both hard stroke (i.e., displacement) limits and force ratings. The approach models the WEC dynamics in discrete-time, in a manner that exactly preserves energy-flow quantities, and assumes a stationary stochastic disturbance model for the incident wave force. The control objective is to maximize the expected power generation in stationarity, while accounting for parasitic losses in the power train. PTO stroke measurements are assumed to be available for real-time feedback, as well as the free-surface elevation of the waves at a designated location relative to the WEC, and the open-loop dynamics of the WEC are assumed to be linear and time-invariant. Mean-square stability of the MPC algorithm is proven. The methodology is illustrated in a simulation example pertaining to a heaving cylindrical buoy.**

***Index Terms*— Energy Systems, Model Predictive Control, Passivity**

I. Introduction

Wave energy converters have been researched extensively for many decades [1]. The vast array of technologies proposed to harness the resource is diverse and defies easy generalization [2]–[4]. However, most WEC devices are comprised of a mechanical system, either floating at the ocean surface or mounted to the ocean floor, which is dynamically-excited by propagating waves [5]. This mechanical motion is coupled to one or more PTOs (which can be either electromechanical or hydraulic) which extract power from the structural dynamics [6]–[9]. The PTOs are interfaced with a power train that transmits extracted power to a localized storage system (such as a electrical supercapacitor, a flywheel, or a hydraulic accumulator) which serves as a buffer, allowing for smoothed power to be transmitted to a utility grid [10], [11]. To maximize power production in irregular (i.e., stochastic) waves, there is a tangible advantage to the control of the power extracted by the PTOs, based on real-time feedback measurements of the WEC system's dynamic response [12]–[15]. The synthesis of optimal controllers for WEC systems is a topic that continues to be an area of active research.

The first author was supported by an NSF Graduate Research Fellowship. Both authors received further support from NSF grant 2206018. This funding is gratefully acknowledged. Views expressed in this paper are those of the authors and do not necessarily reflect those of the National Science Foundation.

C. Ligeikis is with the Department of Mechanical Engineering, Lafayette College, Easton, PA, USA. J. Scruggs is with the Department of Civil & Environmental Engineering, University of Michigan, Ann Arbor, MI, USA. email: ligeikic@lafayette.edu, jscruggs@umich.edu

Early studies on the optimal control of WECs focused primarily on linear feedback laws. Beginning with the seminal papers by Falnes [16] and Evans [17], it was recognized that in monochromatic waves, power is maximized by imposing an effective impedance relationship between the PTO velocity vector, and the opposing force or torque vector, with the optimal impedance matrix equal to the Hermitian adjoint of the driving point impedance of the WEC system. This result is equivalent to the impedance matching technique used in antenna arrays and other electromagnetic technologies. Impedance matching is of limited practicality for at least three distinct reasons. The first is that, when extended to the case of stochastic waves, the optimal impedance is anti-causal, and therefore can only be implemented if an accurate forecast is available for the incident wave forces [18], [19]. Secondly, the technique presumes that the PTOs have no constraints. This is especially problematic because the dynamic response of the controlled WEC system often deviates further from equilibrium than the uncontrolled system [20]–[22]. As such, it is important to account for constraints on the PTOs, particularly their limits on displacement, and their force ratings. Thirdly, impedance matching does not extend easily to WEC systems with significant nonlinear dynamics [23].

For all these reasons, the last decade has seen a rally around the use of MPC techniques to maximize the energy generated by WEC systems [21], [22], [24]–[29]. MPC is well-suited to address the second problem discussed above, concerning the accommodation of PTO constraints. Additionally, nonlinear MPC techniques exist which may be applied to WEC systems with nonlinear dynamics [30]–[33]. However, most of the MPC techniques implemented for WEC systems do not directly address the first problem, related to causality. Indeed, many techniques assume an accurate real-time prediction exists over a long receding horizon, for the incident wave force. Predicated on this assumption, MPC is implemented at each discrete time step by optimizing the control force/torque trajectory for the PTOs over this receding horizon. The first component of this optimized trajectory is then implemented by the controller. At the next time step, the receding horizon for the wave force forecast is advanced, the control trajectory is re-optimized, and the process is thus repeated ad infinitum.

Many techniques for this have been proposed in the literature to forecast incident wave forces, for use in MPC algorithms. Some obtain the forecast by assuming that measurements of free-surface elevations are available at a distance upwave from the WEC [34]. However, most approaches presume that the incident wave force on the WEC can be measured [35],

and predict the future force trajectories from past data using one of several algorithms, including fully-empirical curve-fitting algorithms as well as model-based algorithms such as the extended Kalman filter [36]–[40].

The primary purpose of this paper is to provide an alternative to the above prediction-based techniques, and to establish that WEC MPC algorithms need not include an explicit wave force forecast at all, to achieve near-optimal performance. Specific contributions of the paper are:

a) We illustrate an entirely causal technique for implementing MPC in WEC applications, which only requires that the power spectral density of the sea state be known.
b) We illustrate that if free surface elevations are measured and available for feedback, these measurements may be systematically incorporated into the MPC algorithm.
c) We illustrate how parasitic losses in the PTO and power train can be systematically incorporated into the MPC optimization objective.
d) We prove that the MPC algorithm is stable in the sense of Lyapunov (for free response), in the bounded-input bounded-state sense (for transient response), and in the mean-square sense (for stochastic response).

The scope of the paper is limited to WEC systems with linear plant dynamics, but many of the techniques we discuss may be extended to the nonlinear case.

The paper is organized as follows. Section II establishes the discrete-time stochastic modeling framework. Section III formalizes the WEC feedback control problem, and establishes the MPC control framework. Section IV focuses on the trajectory optimization problem for the MPC controller, illustrates how this algorithm can be implemented as a convex optimization, and provides the stability results. Section V provides a numerical example of the implementation of the MPC algorithm for a heaving, cylindrical WEC. Finally, Section VI draws some conclusions.

A. Notation and terminology

Sets are denoted in blackboard font, e.g., $\mathbb{R}$, $\mathbb{C}$, $\mathbb{Z}$, and so on. We notate $\mathbb{R}_{\geqslant 0}$ and $\mathbb{Z}_{\geqslant 0}$ as the sets of all nonnegative reals and integers, respectively. The notation $\mathbb{C}_{\leqslant 1}$ (and $\mathbb{C}_{<1}$) denote the complex numbers with moduli less than (strictly less than) 1. Similar definitions hold for the opposite inequalities. For a matrix $Q \in \mathbb{R}^{n\times m}$ or $\mathbb{C}^{n\times m}$, Q^T and Q^H are the transpose and Hermitian transpose, respectively. For a vector $q \in \mathbb{R}^n$ or $\mathbb{C}^n$ and $p \in \mathbb{Z}_{\geqslant 1}$, the norm $\|q\|_p = [\sum_{i=1}^n |q_i|^p]^{1/p}$ and the norm $\|q\|_\infty = \max_i |q_i|$. For a matrix $Q \in \mathbb{R}^{n\times m}$ or $\mathbb{C}^{n\times m}$ and $p \in \mathbb{Z}_{\geqslant 1} \cup \{\infty\}$, the norm $\|Q\|_p$ is the induced norm, i.e., $\sup_{\|q\|_p=1} \|Qq\|_p$. When no subscript is specified for a norm, i.e., $\|\cdot\|$, $p = 2$ is assumed. For a matrix $Q = Q^H \geqslant 0$ and a compatible vector q, we denote $\|q\|_Q = (q^H Q q)^{1/2}$.

For p finite, the set $\mathbb{L}_p$ is the set of all Lebesgue-integrable functions $f(x)$ of a real variable x, such that $\|f\|_{\mathbb{L}_p} \triangleq (\int_{-\infty}^{\infty} \|f(x)\|^p dx)^{1/p} < \infty$. The set $\mathbb{L}_\infty$ is the set of all Lebesgue-integrable functions $f(x)$ such that $\|f\|_{\mathbb{L}_\infty} \triangleq \sup_{x\in\mathbb{R}} \|f(x)\| < \infty$. For a continuous-time function $f(t)$ we denote its Fourier transform as $\hat{f}(j\omega)$. For a discrete-time function f_k, we denote its z-transform as $\bar{f}(z)$. The sets $\mathbb{H}_2$ and $\mathbb{H}_\infty$ are the Hardy spaces, comprised of complex functions $\bar{f}(z)$ which are analytic for all $z \in \mathbb{C}_{>1}$, and which satisfy an appropriate norm on the boundary. For $\bar{f} \in \mathbb{H}_2$, we require that $\|\bar{f}\|_{\mathbb{H}_2} \triangleq (\frac{1}{2\pi}\int_{-\pi}^{\pi} \|\bar{f}(e^{j\Omega}\|^2 d\Omega)^{1/2} < \infty$. For $\bar{f} \in \mathbb{H}_\infty$ we require that $\|\bar{f}\|_{\mathbb{H}_\infty} \triangleq \sup_{\Omega\in[-\pi,\pi]} \|\bar{f}(e^{j\Omega})\|^2 < \infty$.

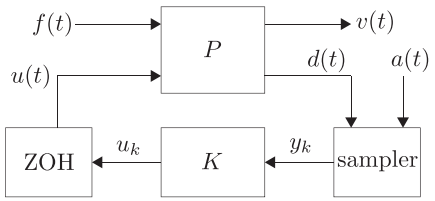

Fig. 1. System block diagram

Stochastic processes and sequences, and other random variables, are denoted in bold. For a random variable $\boldsymbol{x}$, a particular realization is denoted by the same character in italics, i.e., x. For a random variable $\boldsymbol{x}$ and information $\mathbb{I}$, we denote $\mathcal{E}\{\boldsymbol{x}|\mathbb{I}\}$ as the conditional expectation of $\boldsymbol{x}$. For two random variables $\boldsymbol{x}$ and $\boldsymbol{y}$, the expression $\mathcal{E}\{\boldsymbol{y}|\boldsymbol{x}\}$ is $\boldsymbol{y}$ conditioned on $\boldsymbol{x}$, and should be interpreted as a function of random variable $\boldsymbol{x}$. With reference to a stochastic sequence $\{\boldsymbol{x}_k : k \in \mathbb{Z}\}$ we refer to a particular realization of a component or sub-sequence as *data*. The abbreviations wp1 and a. s. stand for "with probability 1" and "almost sure."

II. System Modeling

A. Continuous-time model

For a WEC system with n_p PTOs, let $\boldsymbol{d}(t) \in \mathbb{R}^{n_p}$ be the vector of PTO displacements, and let $\boldsymbol{v}(t) \triangleq \frac{d}{dt}\boldsymbol{d}(t)$ be the resultant velocity vector. Further, let $\boldsymbol{u}(t) \in \mathbb{R}^{n_p}$ be the vector of colocated forces (or torques) associated with the PTOs. We assume that $\boldsymbol{u}(t)$ can be made to track a command with high bandwidth, and therefore can be treated as an input that can be controlled directly. Let $\boldsymbol{f}(t) \in \mathbb{R}^{n_f}$ be the vector of forces on the various mechanical degrees of freedom of the WEC system, due to the incident waves. Let $\boldsymbol{a}(t) \in \mathbb{R}$ be the free surface elevation at some fixed location in the ocean, not necessarily colocated with the location of the WEC system. The structure of the feedback system we consider is shown in Fig. 1. Plant P is comprised of the WEC and surrounding fluid, and is dynamically excited by $\boldsymbol{f}(t)$ and $\boldsymbol{u}(t)$, resulting in outputs $\boldsymbol{d}(t)$ and $\boldsymbol{v}(t)$. Sampled values of $\boldsymbol{d}(t)$ and $\boldsymbol{a}(t)$ are sent to discrete-time controller K, which formulates continuous-time force $\boldsymbol{u}(t)$ via a Zero-Order Hold (ZOH) conversion. Both $\boldsymbol{f}(t)$ and $\boldsymbol{a}(t)$ are stationary stochastic processes with known joint power spectral density.

For the plant P, we presume linear time-invariant (LTI) mappings Z_{fd} and Z_{ud}, such that

$$\boldsymbol{d}(t) = (Z_{fd}\boldsymbol{f})(t) + (Z_{ud}\boldsymbol{u})(t). \tag{1}$$

These mappings are uniquely characterized by their frequency response functions $\hat{Z}_{fd}(j\omega)$ and $\hat{Z}_{ud}(j\omega)$, which are obtained from the hydrodynamic analysis of the WEC. For simple WEC shapes, they can be obtained via analytical series solutions to the partial differential equations characterizing the fluid-structure interaction [41]. For more realistic WEC shapes,

they can be obtained by via finite-element techniques [42]. Regardless of how they are obtained, Z_{fd} and Z_{ud} are in general infinite-dimensional (i.e., their transfer functions are irrational), due to fluid-structure interaction.

Remark 1: In reality all WEC systems exhibit some nonlinear effects, and (1) only approximates the true dynamics of P. Nonetheless, linear models of the form (1) are often used for the purposes of control design [14], [19], [21], [26], including many experimental implementations [27], [43]–[47]. They do not precisely capture the effects of viscous drag [48]. However, for the cylindrical WEC considered in the example for this paper (in which the PTO is fully-encased inside the cylinder) viscous drag forces are of secondary contributor to the overall damping of the WEC system when compared to the (linear) radiation damping forces. Depending on the geometry and kinematics of the WEC, there may also be nonlinear Froude-Krylov forces. However, in many simple WEC systems, including the surface-floating cylindrical WEC considered in the example, nonlinear Froude-Krylov forces are insignificant and can be disregarded [49].

The power spectral density (PSD) of $\boldsymbol{a}$, denoted $S_a(\omega)$, is defined with the convention that

$$\mathcal{E}\left\{\boldsymbol{a}(t+\tau)\boldsymbol{a}(t)\right\} = \frac{1}{2\pi}\int_{-\infty}^{\infty} e^{j\omega\tau} S_a(\omega) d\omega \tag{2}$$

We assume linear wave theory, and consequently, that there exists a (noncausal) LTI deterministic mapping Z_{af} such that

$$\boldsymbol{f}(t) = \left(Z_{af}\boldsymbol{a}\right)(t) \tag{3}$$

where Z_{af} is uniquely characterized by its frequency-response function $\hat{Z}_{af}(j\omega)$, which must also be obtained through hydrodynamic analysis. Letting $\boldsymbol{d}_f(t) \triangleq (Z_{fd}\boldsymbol{f})(t)$, we have that $\boldsymbol{d}_f(t)$ is a stationary stochastic process as well. Defining

$$\boldsymbol{y}_f(t) \triangleq \begin{bmatrix}\boldsymbol{d}_f^T(t) & \boldsymbol{a}(t)\end{bmatrix}^T \tag{4}$$

we have that the joint spectrum of $\boldsymbol{y}_f$ is

$$S_{y_f}(\omega) = \begin{bmatrix}\hat{Z}_{fd}(j\omega)\hat{Z}_{af}(j\omega) \\ 1\end{bmatrix} S_a(\omega) \begin{bmatrix}\hat{Z}_{fd}(j\omega)\hat{Z}_{af}(j\omega) \\ 1\end{bmatrix}^H. \tag{5}$$

The stochastic system model is then, equivalently,

$$\begin{bmatrix}\boldsymbol{d}(t) \\ \boldsymbol{a}(t)\end{bmatrix} = \boldsymbol{y}_f(t) + \begin{bmatrix}I \\ 0\end{bmatrix}\left(Z_{ud}\boldsymbol{u}\right)(t) \tag{6}$$

Recalling that $\boldsymbol{v}(t) = \frac{d}{dt}\boldsymbol{d}(t)$, we have that

$$\boldsymbol{v}(t) = \tfrac{d}{dt}\boldsymbol{d}_f(t) + \left(Z_{uv}\boldsymbol{u}\right)(t) \tag{7}$$

where mapping Z_{uv} is uniquely characterized by its frequency response functions, as

$$\hat{Z}_{uv}(j\omega) = j\omega\hat{Z}_{ud}(j\omega) \tag{8}$$

and where we note that the spectrum for $\frac{d}{dt}\boldsymbol{d}_f$ is $S_{v_f}(\omega) = \omega^2\hat{Z}_{fd}(j\omega)\hat{Z}_{af}(j\omega)S_a(\omega)\hat{Z}_{fd}^H(j\omega)\hat{Z}_{af}^H(j\omega)$.

Remark 2: In the literature on WEC control, it is common to model $\boldsymbol{a}(t)$ as an exogenous input, and to absorb the non-causal transfer function Z_{af} into the plant model P. By contrast, the above approach effectively treats *both* $\boldsymbol{a}(t)$ and $\boldsymbol{f}(t)$ as exogenous stochastic processes with a joint PSD. This approach is equivalent to the more common technique, but circumvents the need for a noncausal plant model.

Remark 3: Because $a(t)$ is presumed to be measured in real-time, our assumption that PSD $S_a(\omega)$ is known is justified. Many spectrum identifications algorithms exist which can be used to identify $S_a(\omega)$ in real-time, from measured data. In particular, we note recent subspace-based algorithms, such as the one proposed in [50], which efficiently identify spectra from time-domain data.

Our development will require certain assumptions to be made for the above model. Here, we state these assumptions in the broadest context for which the theory still applies.

Assumption 1: We assume the following:

a) $\{\hat{Z}_{ud}, \hat{Z}_{uv}\} \subset \mathbb{L}_\infty$ and $\{S_{y_f}, S_{v_f}\} \subset \mathbb{L}_\infty \cap \mathbb{L}_1$.
b) The limit $\hat{Z}_{uv}^\infty \triangleq \lim_{\omega\to\infty}\hat{Z}_{uv}(j\omega)$ exists and is real.
c) Let $\tilde{Z}_{uv}(t)$ be the impulse response of Z_{uv}, i.e.,

$$\tilde{Z}_{uv}(t) = \hat{Z}_{uv}^\infty\delta(t) + \frac{1}{2\pi}\int_{-\infty}^{\infty} e^{j\omega t}\left(\hat{Z}_{uv}(j\omega) - \hat{Z}_{uv}^\infty\right)d\omega \tag{9}$$

with a similar definition for $\tilde{Z}_{ud}(t)$. We assume $\{\tilde{Z}_{uv}, \tilde{Z}_{ud}\} \subset \mathbb{L}_1$.
d) Z_{uv} (and therefore Z_{ud}) are causal mappings, i.e., $\tilde{Z}_{uv}(t) = \tilde{Z}_{ud}(t) = 0$ for all $t < 0$.
e) Z_{uv} is a passive mapping. Equivalently, $\hat{Z}_{uv}$ is positive-real, i.e.,

$$\hat{Z}_{uv}(j\omega) + \hat{Z}_{uv}^H(j\omega) \geqslant 0, \quad \forall\omega \in \mathbb{R} \tag{10}$$

with the inequality holding strictly for all but a countably-finite subset of $\omega \in \mathbb{R}$.

Remark 4: Assumptions 1a, 1b, 1c, and 1d are stated here explicitly, but are taken for granted in most of the literature on WEC control. We note that Assumption 1c implies that the mappings Z_{uv} and Z_{ud} have bounded $\mathbb{L}_\infty$ gain. Because of (8), Assumption 1a necessarily implies that $\hat{Z}_{uv}(0) = 0$, and also that $\hat{Z}_{ud}$ must be strictly proper.

Remark 5: If Assumption 1e is not satisfied, this implies that the WEC possesses an internal energy source. In that case, even in the absence of a disturbance (i.e., with $\boldsymbol{f} = 0$), energy can be generated, implying the WEC is a perpetual-motion machine. The caveat that (10) is strict for all but countably-finite frequencies is mild. At these frequencies, it is possible to excite the WEC with a sinusoidal force $\boldsymbol{u}(t)$ that results in zero mechanical power injection. For almost all applications, the only (finite) frequency where this can occur is $\omega = 0$.

The power generated by the WEC at time t is denoted $\boldsymbol{\varrho}(t)$, and is assumed to be of the form

$$\boldsymbol{\varrho}(t) = -\boldsymbol{u}^T(t)\boldsymbol{v}(t) - \boldsymbol{u}^T(t)R\boldsymbol{u}(t) - v_d^T\left|\boldsymbol{u}(t)\right| \tag{11}$$

where $R \in \mathbb{R}^{n_p\times n_p}$ with $R = R^T > 0$, and $v_d \in \mathbb{R}_{\geqslant 0}^{n_p}$ are parameters. The first term on the right-hand side of (11) is equal to the total power absorbed from the WEC dynamics by the PTO at time t. The second and third terms are used to model transmission losses in the power train between the PTO and the utility bus. For an electrical power train, these two terms capture the conductive power dissipation in the PTO and power electronics, with the second term capturing ohmic (i.e., "I^2R") losses, and the third term capturing diode losses.

B. Energy-preserving discretization

We assume the control input $\boldsymbol{u}(t)$ is implemented as a zero-order hold (ZOH) signal, i.e.,

$$\boldsymbol{u}(t) = \boldsymbol{u}_k, \quad \forall t \in [kT, (k+1)T) \tag{12}$$

where T is the sample time, and $k \in \mathbb{Z}$. We analogously refer to continuous-time signals sampled at the transition times of the ZOH mapping via subscripts, i.e., $\boldsymbol{d}_k = \boldsymbol{d}(kT)$, $\boldsymbol{a}_k = \boldsymbol{a}(kT)$, and so on. Let $\boldsymbol{p}_k$ be the average value of $\boldsymbol{\varrho}(t)$ over the interval $t \in [kT, (k+1)T)$. Then

$$\boldsymbol{p}_k = -\left(\boldsymbol{u}_k^T \boldsymbol{q}_k + \boldsymbol{u}_k^T R \boldsymbol{u}_k + v_d^T \left|\boldsymbol{u}_k\right|\right) \tag{13}$$

where

$$\boldsymbol{q}_k \triangleq \tfrac{1}{T}\left(\boldsymbol{d}_{k+1} - \boldsymbol{d}_k\right). \tag{14}$$

The stochastic dynamics of the resulting sampled continuous-time system can be expressed exactly, as

$$\boldsymbol{d}_k = \left(H_{wd}\boldsymbol{w}\right)_k + \left(H_{ud}\boldsymbol{u}\right)_k \tag{15}$$

$$\boldsymbol{a}_k = \left(H_{wa}\boldsymbol{w}\right)_k \tag{16}$$

where $\boldsymbol{w}_k \in \mathbb{R}^{n_p+1}$ is an independent, identically-distributed Gaussian stochastic sequence with zero-mean and covariance $S_w \succcurlyeq 0$, and mappings H_{wd} and H_{wa} are chosen such that $\boldsymbol{d}_k$ and $\boldsymbol{a}_k$ have probability distributions identical to those of the continuous-time system. Mappings H_{ud}, H_{wd}, and H_{wa} are uniquely characterized by discrete-time frequency response functions $\bar{H}_{ud}(e^{j\Omega})$, $\bar{H}_{wd}(e^{j\Omega})$ and $\bar{H}_{wa}(e^{j\Omega})$. It follows that

$$\boldsymbol{q}_k = \left(H_{wq}\boldsymbol{w}\right)_k + \left(H_{uq}\boldsymbol{u}\right)_k \tag{17}$$

where mappings H_{wq} and H_{uq} are uniquely characterized by their discrete-time frequency response functions

$$\bar{H}_{uq}(e^{j\Omega}) = \tfrac{1}{T}(e^{j\Omega} - 1)\bar{H}_{ud}(e^{j\Omega}) \tag{18}$$

$$\bar{H}_{wq}(e^{j\Omega}) = \tfrac{1}{T}(e^{j\Omega} - 1)\bar{H}_{wd}(e^{j\Omega}) \tag{19}$$

In [51] it was shown that $\bar{H}_{uq}(e^{j\Omega})$, $\Omega \in [-\pi, \pi]$ is

$$\bar{H}_{uq}(e^{j\Omega}) = \sum_{\ell=-\infty}^{\infty} \hat{Z}_{uv}(j\omega_\ell)\,\mathrm{sn}^2(\omega_\ell T/2) \tag{20}$$

where $\omega_\ell \triangleq \Omega/T + 2\pi\ell/T$. $\bar{H}_{ud}(e^{j\Omega})$ is then found via (18). Meanwhile, to get mappings $\bar{H}_{wd}(e^{j\Omega})$ and $\bar{H}_{wa}(e^{j\Omega})$, we first find the discrete-time joint PSD

$$\Sigma_{y_f}(\Omega) = \sum_{\ell=-\infty}^{\infty} \frac{1}{T}\,\mathrm{sn}^2(\omega_\ell T/2) S_{y_f}(\omega_\ell). \tag{21}$$

Then, via the Spectral Factorization Theorem, we find $\bar{H}_{wd}(e^{j\Omega})$ and $\bar{H}_{wa}(e^{j\Omega})$ as causal, minimum-phase, discrete-time frequency-response functions satisfying

$$\Sigma_{y_f}(\Omega) = \begin{bmatrix} \bar{H}_{wd}(e^{j\Omega}) \\ \bar{H}_{wa}(e^{j\Omega}) \end{bmatrix} S_w \begin{bmatrix} \bar{H}_{wd}(e^{-j\Omega}) \\ \bar{H}_{wa}(e^{-j\Omega}) \end{bmatrix}^T. \tag{22}$$

Frequency response function $\bar{H}_{wq}(e^{j\Omega})$ is then found via (19). We note that in (22), the factorization is not unique. Without loss of generality, we adopt the convention of a canonical factorization [52], in which S_w is normalized such that

$$\frac{1}{2\pi}\int_{-\pi}^{\pi} \begin{bmatrix} \bar{H}_{wd}(e^{j\Omega}) \\ \bar{H}_{wa}(e^{j\Omega}) \end{bmatrix} d\Omega = I. \tag{23}$$

Associated z-domain transfer functions $\bar{H}_{uq}(z)$, $\bar{H}_{wq}(z)$, $\bar{H}_{ud}(z)$, $\bar{H}_{wd}(z)$ and $\bar{H}_{wa}(z)$ are obtained by inverse-transforming the discrete-time frequency-response functions to get discrete-time impulse response functions, and then z-transforming these. The following theorem groups together some useful properties of these transfer functions.

Theorem 1: If Assumption 1 holds then:

a) $\{\bar{H}_{uq}, \bar{H}_{ud}\} \in \mathbb{H}_\infty$ and $\{\bar{H}_{wa}, \bar{H}_{wd}\} \subset \mathbb{H}_2 \cap \mathbb{H}_\infty$.

b) $\bar{H}_{uq}$ is positive-real in discrete-time, i.e., it is analytic for all $z \in \mathbb{C}_{>1}$ and satisfies

$$\bar{H}_{uq}(z) + \bar{H}_{uq}^H(z) \geqslant 0, \quad \forall z \in \mathbb{C}_{\geqslant 1} \tag{24}$$

with the inequality holding strictly except for $z = 1$.

c) $\bar{H}_{uq}(1) = 0$, and $\bar{H}_{ud}(1) + \bar{H}_{ud}^H(1) > 0$.

Remark 6: Discrete-time models (15) and (16) *exactly* characterize the stochastic response of the continuous-time dynamic system, under the assumption that $\boldsymbol{u}(t)$ is as in (12). The probabilistic distributions for the discrete-time system model are precisely those that would be obtained by sampling the continuous-time system dynamics. Additionally, (13) is an *exact* expression for the mean power generation over interval $t \in [kT, (k+1)T)$. In the literature on WEC control, it is common to approximate $\boldsymbol{p}_k \approx \boldsymbol{\varrho}_k$ [53], which is inexact. (It is this distinction that justifies the usage of the term "energy-preserving" for our discretization procedure.) Although this distinction may at first appear subtle, it can have significant consequences for the well-posedness of the discrete-time MPC algorithm, because if the energy-preserving discretization is not used, properties (b) and (c) of Theorem 1 may not hold.

C. Finite-dimensional discrete-time model

Because the continuous-time system exhibits infinite-dimensional dynamics, the discrete-time models (15) and (16) do as well. In order to apply MPC, H_{ud}, H_{wd}, and H_{wa} must be approximated as finite-dimensional, LTI, discrete-time systems, using any of several system identification techniques. Let $\boldsymbol{y} \triangleq [\boldsymbol{d}^T \ \boldsymbol{a}]^T$. Without loss of generality we assume the resulting state space system for the mapping $\{\boldsymbol{u}, \boldsymbol{w}\} \mapsto \boldsymbol{y}$ is in the form of an innovations model [54], i.e.,

$$H : \left\{ \begin{array}{rl} \boldsymbol{x}_{k+1} = & A\boldsymbol{x}_k + B_u\boldsymbol{u}_k + B_w\boldsymbol{w}_k \\ \boldsymbol{y}_k = & C_y\boldsymbol{x}_k + \boldsymbol{w}_k \end{array} \right. \tag{25}$$

and a minimal realization[1]. For convenience, define partitions

$$C_y = \begin{bmatrix} C_d \\ C_a \end{bmatrix}, \quad I = \begin{bmatrix} D_{wd} \\ D_{wa} \end{bmatrix} \tag{26}$$

and note that

$$\bar{H}_{ud}(z) \approx C_d\left[zI - A\right]^{-1} B_u \tag{27}$$

$$\bar{H}_{wd}(z) \approx D_{wd} + C_d\left[zI - A\right]^{-1} B_w \tag{28}$$

$$\bar{H}_{wa}(z) \approx D_{wa} + C_a\left[zI - A\right]^{-1} B_w. \tag{29}$$

Furthermore, $\boldsymbol{q}_k$ is

$$\boldsymbol{q}_k = C_q\boldsymbol{x}_k + D_{uq}\boldsymbol{u}_k + D_{wq0}\boldsymbol{w}_k + D_{wq1}\boldsymbol{w}_{k+1} \tag{30}$$

[1]Note that, as with all innovations models, the state vector $\boldsymbol{x}_k$ should not be thought of as a physical state, but rather, as the optimal state estimate for the system, conditioned on $\{\boldsymbol{y}_\ell, \ell < k\}$. Model (25) can equivalently be viewed as a Kalman filter, with matrix B_w as the associated Kalman gain.

where

$$C_q = \tfrac{1}{T} C_d (A - I), \qquad D_{uq} = \tfrac{1}{T} C_d B_u \tag{31}$$

$$D_{wq0} = \tfrac{1}{T}(C_d B_w - D_{wd}), \qquad D_{wq1} = \tfrac{1}{T} D_{wd} \tag{32}$$

Consequently, we may express transfer functions $\bar{H}_{uq}$ and $\bar{H}_{wq}$ in terms of the state space parameters as

$$\bar{H}_{uq}(z) \approx D_{uq} + C_q [zI - A]^{-1} B_u \tag{33}$$

$$\bar{H}_{wq}(z) \approx D_{wq1} z + D_{wq0} + C_q [zI - A]^{-1} B_w. \tag{34}$$

We presume that the finite-dimensional model has been found in a way that preserves the properties listed in Theorem 1 for the above transfer functions. More information on subspace-based procedures to achieve this can be found in [55] and [56]. The following theorem groups together some useful implications of Theorem 1, which apply to the finite-dimensional model H as in (25).

Theorem 2: Assume the minimal finite-dimensional model (25) is such that the transfer functions (27), (28), (29), and (33) adhere to the conditions in Theorem 1. Then:

a) A is Schur.
b) $D_{uq} + D_{uq}^T > 0$.
c) The discrete-time Riccati equation

$$W = A^T W A + F^T M F \tag{35}$$

with

$$M \triangleq R + \tfrac{1}{2}(D_{uq} + D_{uq}^T) - B_u^T W B_u \tag{36}$$

$$F \triangleq -M^{-1} \left[\tfrac{1}{2} C_q - B_u^T W A \right] \tag{37}$$

has a solution $W = W^T \geqslant 0$ with $M > 0$, and such that $A + B_u F$ is Schur.

Remark 7: Note that, through the process of discretization shown above, the properties in Theorem 2 for dynamic model (25) follow directly from Assumption 1 for the continuous-time system. Properties (a), (b), and (c) are used extensively throughout the remainder of the paper.

D. Inverse system dynamics

Consider the inverse system in which $\boldsymbol{d}$ is treated as a control input, and $\boldsymbol{u}$ is treated as an output. Then

$$\begin{aligned} \boldsymbol{u}_k = &- D_{uq}^{-1} C_q \boldsymbol{x}_k - \tfrac{1}{T} D_{uq}^{-1} (C_d B_w - D_{wd}) \boldsymbol{w}_k \\ &- \tfrac{1}{T} D_{uq}^{-1} D_{wd} \boldsymbol{w}_{k+1} + \tfrac{1}{T} D_{uq}^{-1} (\boldsymbol{d}_{k+1} - \boldsymbol{d}_k). \end{aligned} \tag{38}$$

As such,

$$\begin{aligned} \boldsymbol{x}_{k+1} = &\left[A - B_u D_{uq}^{-1} C_q \right] \boldsymbol{x}_k + \left[\tfrac{1}{T} B_u D_{uq}^{-1} \right] (\boldsymbol{d}_{k+1} - \boldsymbol{d}_k) \\ &+ \tfrac{1}{T} B_u D_{uq}^{-1} D_{wd} (\boldsymbol{w}_k - \boldsymbol{w}_{k+1}) \\ &+ [I - \tfrac{1}{T} B_u D_{uq}^{-1} C_d] B_w \boldsymbol{w}_k. \end{aligned} \tag{39}$$

Changing coordinates, define $\boldsymbol{\zeta}_k$ such that

$$\begin{bmatrix} \boldsymbol{d}_k \\ \boldsymbol{\zeta}_k \end{bmatrix} = \begin{bmatrix} C_d \\ B_u^\perp \end{bmatrix} \boldsymbol{x}_k + \begin{bmatrix} D_{wd} \\ 0 \end{bmatrix} \boldsymbol{w}_k \tag{40}$$

where $B_u^\perp$ is a full-row-rank matrix such that $B_u^\perp B_u = 0$ and such that $[C_d^T \ (B_u^\perp)^T]$ is square and invertible. (Note that this is assumed without loss of generality, because $C_d B_u = T D_{uq}$ is nonsingular.) Then we have that

$$\begin{bmatrix} C_d \\ B_u^\perp \end{bmatrix}^{-1} = \begin{bmatrix} B_u & C_d^\perp \end{bmatrix} \begin{bmatrix} C_d B_u & 0 \\ 0 & B_u^\perp C_d^\perp \end{bmatrix}^{-1} \tag{41}$$

where $C_d^\perp$ is any full-column rank matrix such that $C_d C_d^\perp = 0$ and such that $[B_u \ C_d^\perp]$ is square. Using these facts, it is straight-forward to verify that in the new coordinates,

$$\boldsymbol{\zeta}_{k+1} = A_s \boldsymbol{\zeta}_k + B_{ws} \boldsymbol{w}_k + B_{ds} \boldsymbol{d}_k \tag{42}$$

$$\boldsymbol{x}_k = C_s \boldsymbol{\zeta}_k + D_{ws} \boldsymbol{w}_k + D_{ds} \boldsymbol{d}_k \tag{43}$$

where

$$A_s \triangleq B_u^\perp A C_s \tag{44}$$

$$B_{ws} \triangleq B_u^\perp B_w - B_{ds} D_{wd}, \qquad B_{ds} \triangleq B_u^\perp A D_{ds} \tag{45}$$

$$C_s \triangleq C_d^\perp \left[B_u^\perp C_d^\perp \right]^{-1} \tag{46}$$

$$D_{ws} \triangleq -D_{ds} D_{wd}, \qquad D_{ds} \triangleq \tfrac{1}{T} B_u D_{uq}^{-1} \tag{47}$$

We conclude this section with a theorem which has important implications for the proof of Theorem 5.

Theorem 3: Theorems 1 and 2 imply that A_s is Schur.

III. Optimal Stochastic WEC Control

Let $\boldsymbol{Y}_k$ be

$$\boldsymbol{Y}_k \triangleq \{ \boldsymbol{y}_\ell : \ell < k \} \tag{48}$$

Then we presume that at time k, the information available for the purposes of control is $\boldsymbol{Y}_k$, i.e., we presume a control algorithm K that facilitates the mapping

$$K : \boldsymbol{Y}_k \mapsto \boldsymbol{u}_k \tag{49}$$

for each $k \in \mathbb{Z}_{\geqslant 0}$, starting from a deterministic initial condition $\boldsymbol{x}_0 = x_0$. Random variables $\boldsymbol{x}_k$ and $\boldsymbol{u}_k$ are functions of $\boldsymbol{Y}_k$. At time k the data $\boldsymbol{Y}_k = Y_k$ is known to the control algorithm K, and consequently the data $\boldsymbol{x}_k = x_k$ and $\boldsymbol{u}_k = u_k$ are known. With each time advancement of $k \to k+1$, innovations data $\boldsymbol{w}_k = w_k$ becomes known, and data $\boldsymbol{x}_{k+1} = x_{k+1}$ is evaluated recursively by control algorithm K, via (25).

Let $\mathbb{K}_c$ be the set of all strictly causal mappings K as in (49). The idealized optimal WEC control problem is then

$$K = \text{sol} \left\{ \begin{array}{rl} \text{Given}: & A, B_u, B_w, C_y, S_w, x_0 \\ \text{Max}: & p_{\text{avg}} \\ \text{Dom}: & K \in \mathbb{K}_c \\ \text{Constr}: & |\boldsymbol{u}_k| \leqslant u_{\max} \text{ wp1}, \ \forall k \in \mathbb{Z}_{\geqslant 0} \\ & |\boldsymbol{d}_k| \leqslant d_{\max} \text{ wp1}, \ \forall k \in \mathbb{Z}_{>0} \end{array} \right. \tag{50}$$

where $u_{\max}$ and $d_{\max}$ are the vectors of force and displacement limits, and p_{avg} is the expected mean value of $\boldsymbol{p}$, i.e.,

$$p_{\text{avg}} \triangleq \lim_{\tau \to \infty} \frac{-1}{\tau + 1} \sum_{k=0}^{\tau} \mathcal{E} \left\{ \boldsymbol{u}_k^T C_q \boldsymbol{x}_k + \boldsymbol{u}_k^T \tilde{R} \boldsymbol{u}_k + v_d^T |\boldsymbol{u}_k| \right\} \tag{51}$$

where $\tilde{R} \triangleq R + \frac{1}{2}(D_{uq} + D_{uq}^T) > 0$. Optimization (50) is not well-posed, because for each time k, there is a nonzero probability that there will exist no control input that can simultaneously satisfy both the displacement and force constraints.

To rectify this, we soften the force constraint using a vector of slack variables, denoted $\boldsymbol{b} \in \mathbb{R}^{n_p}_{\geqslant 0}$, giving the relaxed problem

$$K = \text{sol}\left\{\begin{array}{rl} \text{Given}: & A, B_u, B_w, C_y, S_w, x_0 \\ \text{Max}: & p_{\text{avg}} - \lim\limits_{\tau\to\infty} \frac{1}{\tau+1} \sum_{k=0}^{\tau} \mathcal{E}\left\{\mu u_{\max}^T \boldsymbol{b}_k\right\} \\ \text{Dom}: & K \in \mathbb{K}_c \\ \text{Constr}: & |\boldsymbol{u}_k| \leqslant u_{\max} + \boldsymbol{b}_k \,\text{wp1},\ \forall k \in \mathbb{Z}_{\geqslant 0} \\ & |\boldsymbol{d}_k| \leqslant d_{\max}\,\text{wp1},\ \forall k \in \mathbb{Z}_{>0} \\ & \boldsymbol{b}_k \geqslant 0\,\text{wp1},\ \forall k \in \mathbb{Z}_{\geqslant 0} \end{array}\right. \tag{52}$$

where $\mu \in \mathbb{R}_{>0}$ is a penalty term.

The following theorem is instrumental to the formulation of this control problem in the context of MPC.

Theorem 4: Let $K \in \mathbb{K}_c$ be such that the limit

$$\lim_{k\to\infty} \frac{1}{k} \mathcal{E}\left\{\|\boldsymbol{x}_k\|^2\right\} = 0 \tag{53}$$

Then

$$p_{\text{avg}} = \bar{p} - \lim_{\tau\to\infty} \frac{1}{\tau+1} \sum_{k=0}^{\tau} \mathcal{E}\left\{\|\boldsymbol{\xi}_k\|_M^2 + v_d^T |\boldsymbol{u}_k|\right\} \tag{54}$$

where $\boldsymbol{\xi}_k \triangleq \boldsymbol{u}_k - F\boldsymbol{x}_k$, matrices M is as F are defined in (36) and (37), $\bar{p} \triangleq \text{tr}\{B_w^T W B_w S_w\}$, and $W = W^T \geqslant 0$ is the unique stabilizing solution to (35).

Using this theorem, we can re-express the control problem for K as the equivalent problem below:

$$K = \text{sol}\left\{\begin{array}{rl} \text{Given}: & A, B_u, B_w, C_y, S_w, x(0) \\ \text{Min}: & \lim\limits_{\tau\to\infty} \frac{1}{\tau+1} \sum\limits_{k=0}^{\tau} \mathcal{E}\left\{J(\boldsymbol{x}_k, \boldsymbol{u}_k, \boldsymbol{b}_k)\right\} \\ \text{Dom}: & K \in \mathbb{K}_c \\ \text{Constr}: & |\boldsymbol{u}_k| \leqslant u_{\max} + \boldsymbol{b}_k \,\text{wp1}, \forall k \in \mathbb{Z}_{\geqslant 0} \\ & |\boldsymbol{d}_k| \leqslant d_{\max}\,\text{wp1}, \forall k \in \mathbb{Z}_{>0} \\ & \boldsymbol{b}_k \geqslant 0\,\text{wp1},\ \forall k \in \mathbb{Z}_{\geqslant 0} \end{array}\right. \tag{55}$$

where $J(x_k, u_k, b_k)$ is equal to

$$J(x_k, u_k, b_k) \triangleq \|u_k - Fx_k\|_M^2 + v_d^T |u_k| + \mu u_{\max}^T b_k \tag{56}$$

Remark 8: Note that because $M > 0$ and $\mu > 0$, J is a positive-semidefinite, and is convex. This is of central importance in the next section on the MPC formulation, because it implies that the associated real-time optimization executed by the MPC algorithm is convex.

Remark 9: Technically, the optimal control problem (55) is not well-posed. Satisfaction of constraint $|\boldsymbol{d}_k| \leqslant d_{\max}$ must be enforced at previous time step, $k-1$, by appropriate choice of $\boldsymbol{u}_{k-1}$. Ensuring this requires precise knowledge of $\boldsymbol{w}_k$, $\boldsymbol{w}_{k-1}$ and $\boldsymbol{x}_{k-1}$. Due to the fact that K is constrained to be strictly causal, this knowledge is not available until after input $\boldsymbol{u}_{k-1}$ has been applied. As such, there is a finite (albeit very small, in practice) probability of displacement violation, which is unavoidable. To make (55) well-posed, the displacement constraint is relaxed to a conditional expectation, as

$$|\mathcal{E}\left\{\boldsymbol{d}_{k+1} \mid \boldsymbol{Y}_k\right\}| \leqslant d_{\max}\,\text{wp1}, \forall k \in \mathbb{Z}_{\geqslant 0}. \tag{57}$$

IV. MPC Formulation

To frame the optimal stochastic WEC control problem in the context of MPC, suppose the present time is k, data $\boldsymbol{Y}_k = Y_k$ is known. (It follows that data $\boldsymbol{x}_k = x_k$ is also known.) Let $h > 0$ be some receding horizon length, and define

$$\boldsymbol{U}_k \triangleq \{\boldsymbol{u}_k, ..., \boldsymbol{u}_{k+h}\} \tag{58}$$

and let

$$U_{k|k} \triangleq \{u_{k|k}, ..., u_{k+h|k}\} \tag{59}$$

be a sequence of hypothetical, deterministic future control inputs, which are determined from data Y_k and are therefore probabilistically independent of innovations $\{\boldsymbol{w}_k, ..., \boldsymbol{w}_{k+h}\}$. Let $\{x_{k|k}, ..., x_{k+h|k}\}$ be the expected values of $\{\boldsymbol{x}_k, ..., \boldsymbol{x}_{k+h}\}$ conditioned on data Y_k and $U_{k|k}$, i.e.,

$$x_{m|k} \triangleq \mathcal{E}\left\{\boldsymbol{x}_m \middle| \boldsymbol{Y}_k = Y_k, \boldsymbol{U}_k = U_{k|k}\right\} \tag{60}$$

Then it follows that for $m \in \{k, ..., k+h\}$,

$$x_{m+1|k} = Ax_{m|k} + B_u u_{m|k} \tag{61}$$

with initial condition $x_{k|k} = x_k$.

In the proposed stochastic MPC formulation of the optimal control problem, at each time k we find a deterministic input sequence $U_{k|k}$ and a deterministic slack variable sequence

$$B_{k|k} \triangleq \{b_{k|k}, ..., b_{k+h,k}\} \tag{62}$$

which minimize an objective $\Gamma(x_k, U_{k|k}, B_{k|k})$, subject to constraints. As such, we have that

$$u_k = \underset{u_{k|k}}{\text{sol}}\left\{\begin{array}{rl} \text{Given:} & x_k \\ \text{Min:} & \Gamma(x_k, U_{k|k}, B_{k|k}) \\ \text{Dom:} & U_{k|k}, B_{k|k} \\ \text{Constr:} & \Theta(x_k, U_{k|k}, B_{k|k}) \leqslant 0 \\ & \Psi(x_k, U_{k|k}) = 0 \end{array}\right. \tag{63}$$

for appropriately-defined constraint vector functions $\Theta(\cdot,\cdot,\cdot)$ and $\Psi(\cdot,\cdot)$. Let the resultant optimized trajectories be denoted by ring accents, i.e., $\mathring{U}_{k|k} = \{\mathring{u}_{k|k}, ..., \mathring{u}_{k+h|k}\}$ and $\mathring{B}_{k|k} = \{\mathring{b}_{k|k}, ..., \mathring{b}_{k+h|k}\}$. Upon solving this optimization, the MPC algorithm implements $u_k = \mathring{u}_{k|k}$. Following this, data $\boldsymbol{y}_k = y_k$ is obtained, and innovations data $\boldsymbol{w}_k = w_k$ and state data $\boldsymbol{x}_{k+1} = x_{k+1}$ are found from (25). Time is incremented, i.e., $k \to k+1$, and the process is repeated ad infinitum.

Remark 10: Several variants of the stochastic MPC framework exist (see, e.g., [57] and the many references therein). However, almost universally, stochastic MPC algorithms minimize the expectation of a receding-horizon control objective function (e.g., Γ), subject to constraints. Variants differ in two main aspects: (a) the way they impose constraints, and (b) the parametrization of receding-horizon control policies. Regarding aspect (a), constraints are often imposed probabilistically (i.e., as chance constraints), rather than deterministically as they are here. Regarding aspect (b), many methods assume (as we have) that the control input $\boldsymbol{U}_k = U_{k|k}$ is a deterministic trajectory over the receding horizon. Other techniques assume that for $\ell \in \{k, ..., k+h\}$, $\boldsymbol{u}_{\ell|k}$ is a feedback function of $\boldsymbol{x}_\ell$, i.e., $\boldsymbol{u}_\ell = \pi_{\ell|k}(\boldsymbol{x}_\ell)$ for some parametrized class of feedback policies $\pi_{\ell|k}(\cdot)$. Real-time optimization of general

feedback policies is generally intractable except if they have a very simple parametric structure, such as $\pi_{\ell|k}(\boldsymbol{x}_\ell) = u_{\ell|k} + K_{\ell|k}(\boldsymbol{x}_\ell - x_{\ell|k})$ where the optimization variables at each time step of the receding horizon are $u_{\ell|k}$ and $K_{\ell|k}$. In many stochastic MPC variants, $K_{\ell|k}$ is chosen to be time-invariant (i.e., $K_{\ell|k} = K$) and is chosen to stabilize $A + B_u K$, leaving $U_{k|k}$ as the only variables to be optimized in real-time. Here, since A is known to be Schur, we take $K = 0$. This results in a highly-efficient real-time optimization algorithm.

A. Optimization objective

The MPC optimization objective involves the expected value of $J(\boldsymbol{x}_m, u_{m|k}, b_{m|k})$ for $m \in \{k, ..., k+h\}$, conditioned on data $\boldsymbol{Y}_k = Y_k$ as well as $\boldsymbol{U}_k = U_{k|k}$. Because $J(\cdot,\cdot,\cdot)$ is quadratic its first argument, the second and third arguments are deterministic when conditioned on the data, and because $x_{m|k}$ is an unbiased conditional estimate of $\boldsymbol{x}_m$, it follows that

$$\begin{aligned}&\mathcal{E}\left\{ J(\boldsymbol{x}_m, u_{m|k}, b_{m|k}) \middle| \boldsymbol{Y}_k = Y_k, \boldsymbol{U}_k = U_{k|k} \right\} \\ &\quad = \mathcal{E}\left\{ \|F(\boldsymbol{x}_m - x_{m|k})\|_M^2 \right\} + J(x_{m|k}, u_{m|k}, b_{m|k}). \end{aligned} \tag{64}$$

The MPC optimization objective is the sum of this expectation over the time horizon, plus a final-value penalty. Noting that $\boldsymbol{x}_m - x_{m|k}$ is zero for $m = k$ and a linear combination of $\{\boldsymbol{w}_k, ..., \boldsymbol{w}_{m-1}\}$ for $m > k$, it follows that the first term on the right-hand side of (64) is independent of optimization variables $U_{k|k}$ and $B_{k|k}$, and can be subtracted from the objective without affecting the solution. In so doing, the objective to be minimized in the MPC algorithm is

$$\begin{aligned}&\Gamma(x_k, U_{k|k}, B_{k|k}) \\ &\qquad \triangleq J_f(x_{k+h+1|k}) + \sum_{m=k}^{k+h} J(x_{m|k}, u_{m|k}, b_{m|k}) \end{aligned} \tag{65}$$

where for $m \in \{k, ..., k+h\}$, (61) is tacitly assumed, with initial condition $x_{k|k} = x_k$. Term $J_f(\cdot)$ is the final-value penalty, which will be formulated in Section IV-C.

B. Constraints

Inequality constraint vector $\Theta(x_k, U_{k|k}, B_{k|k})$ is formulated to impose the constraints on force, displacement, and the slack variables. Specifically, we have that

$$\Theta(x_k, U_{k|k}, B_{k|k}) = \begin{bmatrix} |u_{k|k}| - b_{k|k} - u_{\max} \\ |d_{k+1|k}| - d_{\max} \\ -b_{k|k} \\ \vdots \\ |u_{k+h|k}| - b_{k+h|k} - u_{\max} \\ |d_{k+h|k}| - d_{\max} \\ -b_{k+h|k} \end{bmatrix} \tag{66}$$

where

$$d_{m|k} \triangleq \mathcal{E}\left\{ \boldsymbol{d}_m | \boldsymbol{Y}_k = Y_k, \boldsymbol{U}_k = U_{k|k} \right\} = C_d x_{m|k} \tag{67}$$

with (61) tacitly assumed with initial condition $x_{k|k} = x_k$.

Equality constraint vector $\Psi(x_k, U_{k|k})$ plays an important role in guaranteeing closed-loop stability of the MPC algorithm. Specifically we impose the condition

$$d_{k+h+1|k} = 0. \tag{68}$$

As such, $\Psi(x_k, U_{k|k}) = C_d x_{k+h+1|k}$, with (61) tacitly assumed with initial condition $x_{k|k} = x_k$.

C. Final value penalty

Due to the imposition of equality constraint (68), it is known for all $U_{k|k}$ satisfying the constraints of MPC algorithm (63), $d_{k+h+1|k} = 0$. Now, let hypothetical inputs $u_{m|k}$ beyond the time horizon, i.e., for $m > k+h$, be those that maintain $d_{m+1|k} = 0$. Using Section II-D, this implies post-horizon trajectories for $x_{m|k}$ and $u_{m|k}$ as

$$x_{m|k} = C_s A_s^{m-(k+h+1)} B_u^{\perp} x_{k+h+1|k} \tag{69}$$

$$u_{m|k} = -D_{uq}^{-1} C_q x_{m|k}. \tag{70}$$

An associated feasible post-horizon penalty term $b_{m|k}$ can then found for all $m \geqslant k+h+1$ as the minimum value that satisfies the force constraint, i.e.,

$$b_{m|k} = \max\{0, |u_{m|k}| - u_{\max}\}. \tag{71}$$

Now, for $u_{m|k}$, and $b_{m|k}$ equal to (70) and (71) respectively, consider the post-horizon performance measure

$$\rho(x_{k+h+1|k}) \triangleq \sum_{m=k+h+1}^{\infty} J(x_{m|k}, u_{m|k}, b_{m|k}) \tag{72}$$

Ideally, we would use $\rho(\cdot)$ as the final-value penalty $J_f(\cdot)$ in MPC performance measure (65). However, $\rho(x_{k+h+1|k})$ is a complex function of its argument, and in the lemma below, we show that it may be over-bounded by a much simpler function.

Lemma 1: There exists a final-value penalty function $J_f(\cdot)$ of the form

$$J_f(x_{k+h+1|k}) = \|x_{k+h+1|k}\|_{Q_f}^2 + \|C_f x_{k+h+1|k}\|_1 \tag{73}$$

where $C_f \in \mathbb{C}^{n_p \times n}$ and $Q_f \in \mathbb{R}^{n \times n}$ with $Q_f = Q_f^T \geqslant 0$, such that the for all $x_{k+h+1|k} \in \mathbb{R}^n$, the following hold:

$$\rho(x_{k+h+1|k}) \leqslant J_f(x_{k+h+1|k}) \tag{74}$$

$$\begin{aligned}&J_f(x_{k+h+2|k}) + J(x_{k+h+1|k}, u_{k+h+1|k}, b_{k+h+1|k}) \\ &\qquad \leqslant J_f(x_{k+h+1|k}) \end{aligned} \tag{75}$$

where for the second inequality, $x_{m|k}$, $u_{m|k}$, and $b_{m|k}$ are evaluated as in (69), (70), and (71) respectively.

We note that the construction of C_f and Q_f is given explicitly in the proof to Lemma 1, in the appendix.

D. Stability

In this subsection we provide a stability proof for MPC algorithm (63). To be more concise, we introduce the notation

$$\|x\|_{1\tau} \triangleq \sum_{k=0}^{\tau} \|x_k\|_1, \qquad \|x\|_{2\tau} \triangleq \left(\sum_{k=0}^{\tau} \|x_k\|_2^2 \right)^{1/2} \tag{76}$$

with similar notation for norms on subsequences of w. Using this notation, the theorem below distills to several common

notions of stability as special cases. For the case in which $w_k = 0$ for all $k \geqslant 0$ and initial condition $x_0 \neq 0$, the theorem guarantees that $\|x\|_{2\tau}$ is bounded from above as $\tau \to \infty$, thus guaranteeing that $\|x_k\|_2 \to 0$ as $k \to \infty$. This implies asymptotic Lyapunov stability. For the case in which $w_k \neq 0$ for some $k \geqslant 0$, and $x_0 = 0$, the theorem establishes a bound on $\|x\|_{2\tau}$ which is a continuous function of $\|w\|_{1\tau}$ and $\|w\|_{2\tau}$, which may be interpreted as a form of bounded-input bounded-state stability. Furthermore, if $\|\frac{1}{1+\tau}w\|_{1\tau}$ and $\|\frac{1}{1+\tau}w\|_{2\tau}$ have finite upper bounds as $\tau \to \infty$, then the result of the theorem guarantees a bound on $\lim_{\tau\to\infty}\|\frac{1}{1+\tau}x\|_{2\tau}$. This has a relationship to mean-square stability for the stochastic system model, as will be shown in the corollary after the theorem.

Theorem 5: Let $\tau \in \mathbb{Z}_{\geqslant 0}$. Assume that for all $k \in \{0, ...\tau\}$, $K : Y_k \mapsto u_k$ is the MPC algorithm (63). Let w be any input sequence with $\|w_k\|$ bounded for all $k \in \{0, .., \tau\}$ and let x_0 be any bounded initial condition. Then there exist constants $\{\alpha_1..., \alpha_4\} \subset \mathbb{R}_{>0}$ such that

$$\|x\|_{2\tau}^2 \leqslant \alpha_1\|x_0\|_1 + \alpha_2\|x_0\|_2^2 + \alpha_3\|w\|_{1\tau} + \alpha_4\|w\|_{2\tau}^2 \quad (77)$$

For the stochastic model we consider in this paper, the above theorem may be interpreted as follows. Equation (77) holds for all stochastic sequences $\boldsymbol{w} = w$ and all initial conditions $\boldsymbol{x}_0 = x_0$ in the ensemble. Consequently, we have that

$$\tfrac{1}{1+\tau}\|\boldsymbol{x}\|_{2\tau}^2 \leqslant \tfrac{\alpha_1}{1+\tau}\|\boldsymbol{x}_0\|_1 + \tfrac{\alpha_2}{1+\tau}\|\boldsymbol{x}_0\|_2^2 + \tfrac{\alpha_3}{1+\tau}\|\boldsymbol{w}\|_{1\tau} + \tfrac{\alpha_4}{1+\tau}\|\boldsymbol{w}\|_{2\tau}^2 \quad (78)$$

Taking $\tau \to \infty$, we have that

$$\lim_{\tau\to\infty} \tfrac{1}{1+\tau}\|\boldsymbol{x}\|_{2\tau}^2 \leqslant \lim_{\tau\to\infty} \tfrac{1}{1+\tau}\left(\alpha_3\|\boldsymbol{w}\|_{1\tau} + \alpha_4\|\boldsymbol{w}\|_{2\tau}^2\right) \quad (79)$$

But recall that each $\boldsymbol{w}_k$ is an independent, identically-distributed, Gaussian random variable with zero mean and covariance S_w. Via the Strong Law of Large Numbers, we therefore have that the following limits hold:

$$\lim_{\tau\to\infty} \tfrac{\alpha_3}{1+\tau}\|\boldsymbol{w}\|_{1\tau} = \alpha_3 \sum_{i=1}^{n_p} \sqrt{\tfrac{2}{\pi}\hat{e}_i^T S_w \hat{e}_i}, \quad \text{a. s.} \quad (80)$$

$$\lim_{\tau\to\infty} \tfrac{\alpha_4}{1+\tau}\|\boldsymbol{w}\|_{2\tau}^2 = \alpha_4 \operatorname{tr}\{S_w\}, \quad \text{a. s.} \quad (81)$$

We conclude that over the ensemble, there exists a bound N equal to the sum of (80) and (81), such that

$$\lim_{\tau\to\infty} \tfrac{1}{1+\tau}\|\boldsymbol{x}\|_{2\tau}^2 \leqslant N, \quad \text{a. s.} \quad (82)$$

As such, we have that in a stochastic context, MPC feedback law (63) is mean-square stable, almost-surely.

Remark 11: The fact that (82) holds almost-surely is a stronger statement than the assertion that the limit holds with probability 1, and implies that the latter holds as well.

V. Example

Consider the WEC system illustrated in Fig. 2, comprised of a floating, slack-moored, cylindrical buoy, in which a tuned vibration absorber (TVA) is embedded. The TVA is comprised of a mass-spring-dashpot assembly, and the PTO is situated between the mass and the buoy. We presume the mooring system restrains the buoy motion to heave. The dynamics of the mass along the buoy axis, together with the heave motion, comprise a two degree-of-freedom vibratory system.

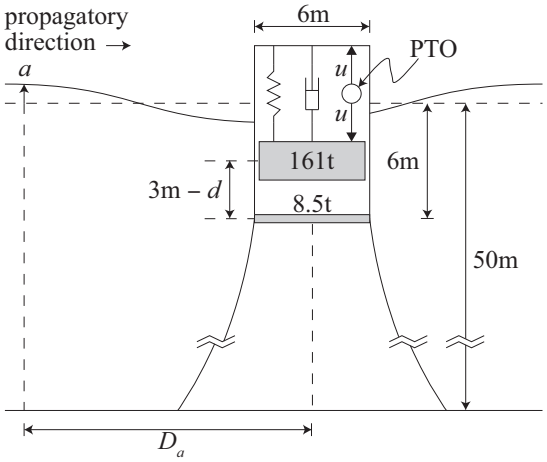

Fig. 2. Example WEC system

The masses of the buoy and TVA were chosen such that the system is in hydrostatic equilibrium in the configuration shown in Fig. 2. The spring of the TVA is such that the fundamental vibratory mode of the system (including the added mass of the displaced fluid) has a natural period of approximately 9s. The dashpot of the TVA is such that the fundamental mode has a fraction of critical damping of 0.5%. Regarding the PTO model, we take $R = 1\text{kW/MN}^2$, and $v_d = 1\text{kW/MN}$. The force and stroke limits are $u_{\max} = 0.5\text{MN}$ and $d_{\max} = 3\text{m}$.

Free surface elevation $a(t)$ is measured at a distance D_a up-wave from the buoy, along the direction of wave propagation. The specific value of D_a will be varied in the example, with $D_a = 0$ implying that measurements are colocated with the buoy. As D_a is increased from 0, the measurements of $a(t)$ can be thought of as providing a kind of preview of the wave loading the buoy will experience in the near-future. However, this is only an approximate interpretation, for two reasons. Firstly, the transfer function from the free surface elevation at the the location of the WEC, to the corresponding wave loading force $f(t)$, is noncausal. Consequently, even if some preview information were available for this free-surface elevation, it would not be possible to exactly determine a preview of $f(t)$. Secondly, ocean waves are dispersive, and consequently waves at different temporal frequencies travel at different velocities. As such, the time history for the free surface elevation at the buoy cannot be viewed simply as a time-delayed version of $a(t)$ at location $D_a > 0$. Despite these two caveats, for the limiting case of $D_a \to \infty$, knowledge of $a(\tau)$ for all $\tau < t$ implies knowledge of the future incident wave loading $f(\tau)$ over an arbitrary but finite receding horizon $\tau \in [t, t + t_h]$.

The stochastic sea state was taken to be a Pierson-Moskowitz spectrum [58], i.e.,

$$S_a(\omega) = c_a \left|\tfrac{\omega_p}{\omega}\right|^5 \exp\left\{-\tfrac{5}{4}\left(\tfrac{\omega_p}{\omega}\right)^4\right\} \quad (83)$$

This spectrum is traditionally parametrized by its significant wave height H_s and peak wave period T_p, with $T_p = \frac{2\pi}{\omega_p}$ and $H_s = 4\sigma_a$, and where $\sigma_a^2 = \frac{1}{2\pi}\int_{-\infty}^{\infty} S_a(\omega)d\omega$. We assume $T_p = 9\text{s}$, and assume $H_s = 1\text{m}$ unless otherwise specified.

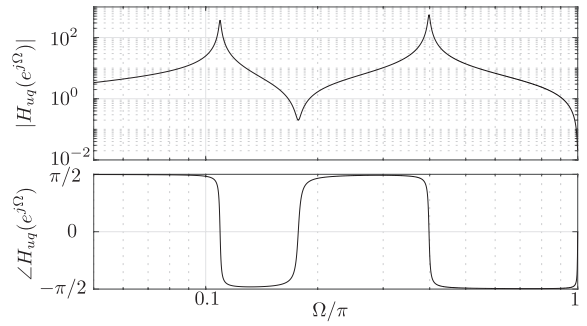

Fig. 3. Frequency response function $\bar{H}_{uq}(e^{j\Omega})$. (Both infinite-dimensional model and finite-dimensional approximation are shown, but are indistinguishable.)

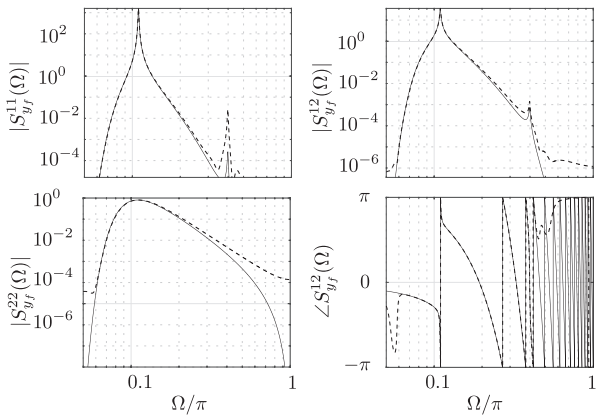

Fig. 4. Spectrum $\boldsymbol{\Sigma_{y_f}(\Omega)}$ for infinite-dimensional model (solid) and finite-dimensional approximation (dashed). Note that $\boldsymbol{S^{11}_{y_f}}$ and $\boldsymbol{S^{22}_{y_f}}$ have zero phase, and $\boldsymbol{S^{21}_{y_f}}$ and $\boldsymbol{S^{12}_{y_f}}$ are complex conjugates.

The sample time for the controller is uniformly taken to be $T = 0.5$s. Fig. 3 shows the discrete-time frequency response function $\bar{H}_{uq}(e^{j\Omega})$, both for the original infinite-dimensional model (as in Section II-B) and the finite-dimensional approximation (as in Section II-C). Note that the both the infinite-dimensional and finite-dimensional models are positive-real. Analogously, Fig. 4 shows the discrete-time spectrum $\Sigma_{y_f}(\Omega)$, both for the infinite-dimensional model and the finite-dimensional approximation, showing a good match at all frequencies where the spectrum magnitude is significant. (This spectrum corresponds to $D_a = 20$m.)

MPC algorithm (63) was implemented for this model, with a time horizon of one minute (i.e., $h = 120$). The only other parameter necessary to specify is the slack penalty factor μ. Performance was found to be insensitive to this value, so long as it is sufficiently large to prohibit violations of the force constraint, and a value of $\mu = 10$ was used for all simulations. All simulations were performed in Matlab, and the optimizations were implemented using CVX [59].

Fig. 5a shows the a sample path realization of the stochastic response of the WEC for the case with $D_a = 0$m. Note that both the force and stroke constraints are uniformly satisfied, as desired. The generated power p_k is also shown. Note that the MPC algorithm requires significant bi-directional power flow (i.e., both significantly positive and significantly negative values). Fig. 5b shows analogous plots for the same case but with $H_s = 3$m. Note that although the average force magnitude is higher than in the $H_s = 1$m case, the force rating is only violated very occasionally, corresponding to times when it is infeasible for the MPC algorithm to simultaneously satisfy both the stroke and force constraints.

To estimate the performance p_{avg} achieved by controller, an ensemble of 48 sample path realizations was simulated for one hour each. The value of p_k was evaluated for each trajectory, resulting in a sample set of 48 values. From this sample set, the p_{avg} was estimated, and confidence intervals were found. The resultant estimates are shown in Fig. 6 for $H_s = 1$m, and for various values of D_a. As D_a is increased, the generated power also increases, asymptotically approaching a limit.

Also shown on the plot is the anticausal power generation performance, which may be viewed as an upper bound on the performance achievable by MPC when accurate wave forecasts are known over a long time horizon. This was obtained by optimizing p_{avg} for each sample in the sample set, assuming the entire w trajectory is known *a priori*. Additionally, in this case the optimal control trajectory was optimized all at once, rather than in the form of an MPC algorithm. As expected, the anticausal performance exceeds the causal performance for all values of D_a. Theoretically, the anticausal optimal performance should be slightly higher than the asymptote of the causal case, as D_a is made large. This asymptotic discrepancy is due to a small degree of sub-optimality inherent to the MPC algorithm as a consequence of its finite horizon. However, it is worth noting that as D_a becomes large, the anticausal and causal performance estimates are close enough that they are within the margin of error for the simulation.

Finally, we examine the manner in which performance changes with H_s. Fig. 7 shows the estimate for p_{avg} for $D_a = 0$m, as a function of H_s. To illustrate the features of this plot better, p_{avg} is normalized by H_s^2. We see that, when normalized as such, the power generation performance has a peak at approximately $H_s = 0.5$m. Above this wave height, constraints on stroke and force hamper the ability of the WEC to harvest the available energy. Below it, the efficiency of the WEC power train drops significantly due to the $v_d^T|u|$ term in the expression for the parasitic dissipation.

VI. Conclusions

In this paper we have illustrated a systematic technique for synthesizing an MPC algorithm for a stochastically-excited WEC, which adheres to force and stroke constraints whenever possible, is provably stable, and does not require the incident wave force to be forecast explicitly. An interesting extension to this work would be the development of a version of the technique which can accommodate nonlinearities in the WEC dynamics. Other items for further study include the stability and performance robustness of the algorithm, in the presence of uncertainty in the WEC dynamic model.

Appendix

A. Proof of Theorem 1

To begin, we observe that $\bar{H}_{uq}(z)$ is analytic on $\mathbb{C}_{>1}$. Let $u_k^i = \hat{e}_i \delta_k$, where $\hat{e}_i$ is the Cartesian unit vector in the i^{th}

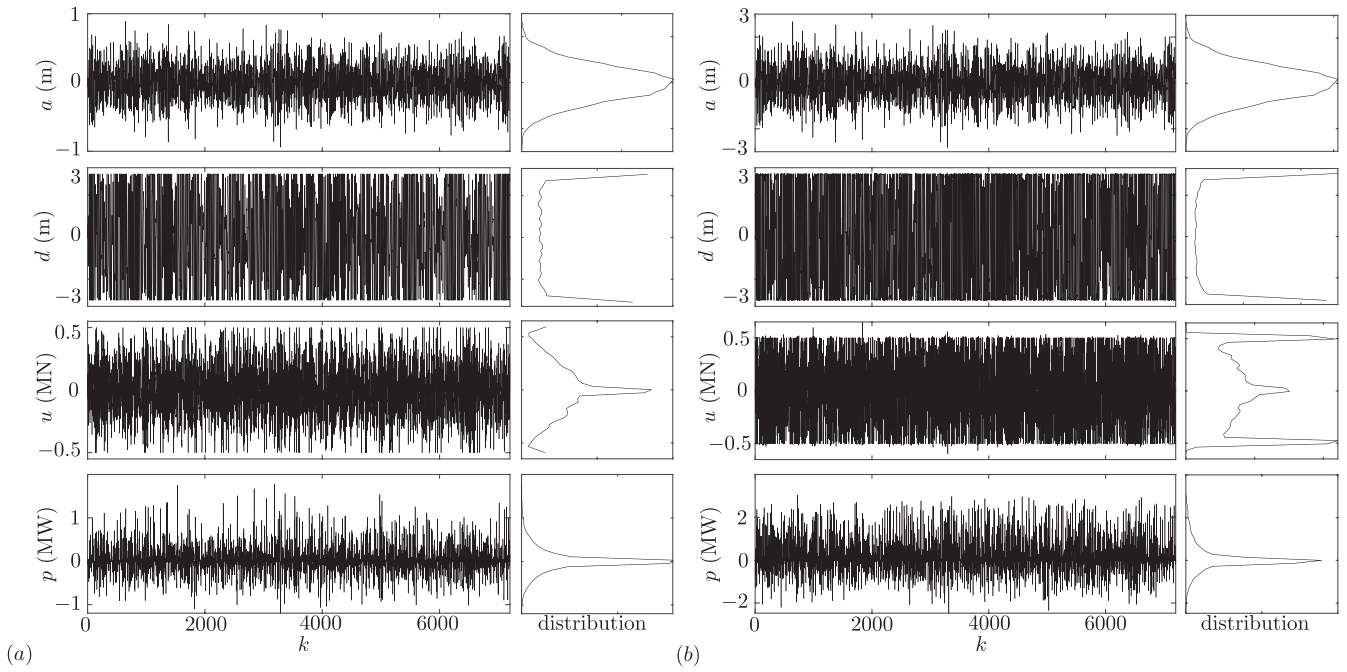

Fig. 5. Sample path realization and distributions for $\boldsymbol{a_k}$, $\boldsymbol{d_k}$, $\boldsymbol{u_k}$, and $\boldsymbol{p_k}$, with MPC algorithm (63), with $\boldsymbol{D_a} = \mathbf{0}$m and $\boldsymbol{H_s} = \mathbf{1}$m (a), and $\mathbf{3}$m (b)

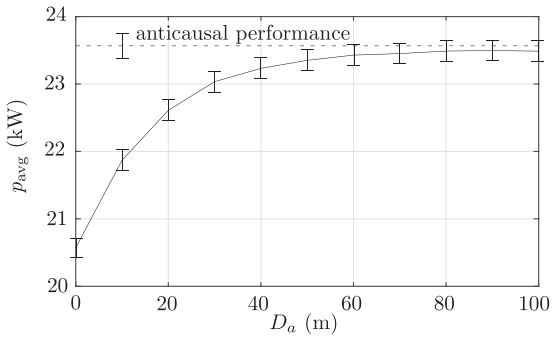

Fig. 6. Estimates of $\boldsymbol{p}_{\text{avg}}$ (with $\mathbf{90\%}$ confidence intervals) vs. $\boldsymbol{D_a}$, with $\boldsymbol{H_s} = \mathbf{1}$m.

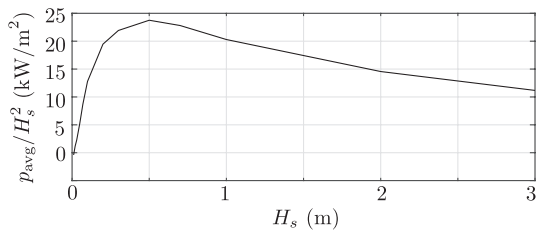

Fig. 7. Estimates of $\boldsymbol{p}_{\text{avg}}$ as a function of $\boldsymbol{H_s}$, with $\boldsymbol{D_a} = \mathbf{0}$m.

direction and δ_k is the Kronecker delta, and let $u^i(t)$ be the resultant continuous-time ZOH input, via (12). Let $v^i(t)$ be the resultant continuous-time response, i.e., $v^i(t) = (Z_{uv}u^i)(t)$. Let q_k^i be the corresponding discrete-time response. Then we note that $\sup_{k\in\mathbb{Z}} \|q_k^i\|_2 \leqslant \|v^i\|_{\mathbb{L}_\infty}$. It is a standard result from input-output analysis that

$$\|v^i\|_{\mathbb{L}_\infty} \leqslant \|\tilde{Z}_{uv}\|_{\mathbb{L}_1}\|u^i\|_{\mathbb{L}_\infty} = \|\tilde{Z}_{uv}\|_{\mathbb{L}_1} \times 1$$

which is finite due to Assumption 1c. We conclude that $\|q_k^i\|_2$ is uniformly bounded for all $k \in \mathbb{Z}_{\geqslant 0}$. Now, consider that $\bar{H}_{uq}(z) = \sum_{k=0}^{\infty} z^{-k}\begin{bmatrix} q_k^1 & \cdots & q_k^{n_p}\end{bmatrix}$ which is analytic if the summation converges. Convergence is guaranteed for $|z| > 1$, due to the uniform bounds on $\|q_k^i\|_2$. We conclude that $\bar{H}_{uq}(z)$ is analytic for $z \in \mathbb{C}_{>1}$. Analogous arguments hold for $\bar{H}_{ud}(z)$. $\bar{H}_{wd}(z)$, and $\bar{H}_{wa}(z)$ are analytic in $\mathbb{C}_{>1}$ by definition, because they are spectral factors.

To prove claim (a), it is already known that each function is analytic for $z \in \mathbb{C}_{>1}$, and it remains to verify that the required frequency-domain norms hold. For $\bar{H}_{uq}$, we require that

$$\|\bar{H}_{uq}\|_{\mathbb{H}_\infty} = \sup_{\Omega\in[-\pi,\pi]} \|\bar{H}_{uq}(e^{j\Omega})\|_2 < \infty.$$

Letting $\sigma_\ell \triangleq \operatorname{sn}(\omega_\ell T/2)$, we have that

$$\|\bar{H}_{uq}(e^{j\Omega})\|_2 = \left\|\sum_{\ell=-\infty}^{\infty} \hat{Z}_{uv}(j\omega_\ell)\sigma_\ell^2\right\|_2 \leqslant \|\hat{Z}_{uv}\|_{\mathbb{L}_\infty}\sum_{\ell=-\infty}^{\infty}\sigma_\ell^2$$

But $\sum_{\ell=-\infty}^{\infty}\sigma_\ell^2 = 1$ so we conclude that $\|\bar{H}_{uq}\|_{\mathbb{H}_\infty} \leqslant \|\hat{Z}_{uv}\|_{\mathbb{L}_\infty}$. Per Assumption 1a, we conclude that $\bar{H}_{uq} \in \mathbb{H}_\infty$. To prove that $\bar{H}_{ud} \in \mathbb{H}_\infty$, we have that

$$\begin{aligned}
\|\bar{H}_{ud}(e^{j\Omega})\|_2 &= \left\|\frac{1}{e^{j\Omega}-1}\sum_{\ell=-\infty}^{\infty}\hat{Z}_{uv}(j\omega_\ell)\sigma_\ell^2\right\|_2 \\
&= \left\|\sum_{\ell=-\infty}^{\infty}\hat{Z}_{ud}(j\omega_\ell)\,|\sigma_\ell|\right\|_2 \\
&\leqslant \left\|\hat{Z}_{ud}(j\omega_0)\right\|_2|\sigma_\ell| + \sum_{\substack{\ell=-\infty\\ \neq 0}}^{\infty}\left\|\hat{Z}_{uv}(j\omega_\ell)\right\|_2\left|\frac{\sigma_\ell}{\omega_\ell}\right| \\
&\leqslant \left\|\hat{Z}_{ud}\right\|_{\mathbb{L}_\infty} + \left\|\hat{Z}_{uv}\right\|_{\mathbb{L}_\infty}\sum_{\ell=1}^{\infty}\frac{T}{(\pi\ell)^2}
\end{aligned}$$

Due to Assumption 1a, the above bound is finite, implying that $\|\bar{H}_{ud}\|_{\mathbb{H}_\infty}$ is finite.

To prove that $\bar{H}_{wa} \in \mathbb{H}_2$, equations (21) and (22) imply

$$2\pi\|\bar{H}_{wa}\|_{\mathbb{H}_2}^2 = \sum_{\ell=-\infty}^{\infty} \int_{-\pi}^{\pi} \frac{1}{T}\sigma_\ell^2 S_a(\omega_\ell)d\Omega \leqslant \int_{-\infty}^{\infty} S_a(\omega)d\omega$$

which is finite due to Assumption 1a. A similar argument proves the same property for $\bar{H}_{wd}$. To prove that $\bar{H}_{wa} \in \mathbb{H}_\infty$, it suffices to show that $\|\bar{H}_{wa}(e^{j\Omega})\|_2$ is uniformly bounded over $\Omega \in [-\pi, \pi]$. Again using (21) and (22),

$$\|\bar{H}_{wa}(e^{j\Omega})\|_2^2 \leqslant \sum_{\ell=-\infty}^{\infty} \frac{1}{T}\sigma_\ell^2 S_a(\omega_\ell) \leqslant \frac{1}{T}\|S_a\|_{\mathbb{L}_\infty}^2$$

which is finite due to Assumption 1a. A similar argument proves the same property for $\bar{H}_{wd}$.

For claim (b), observe that for $\Omega \in [-\pi, \pi]$,

$$\bar{H}_{uq}(e^{j\Omega}) + \bar{H}_{uq}^H(e^{j\Omega}) = \sum_{\ell=-\infty}^{\infty} \left[\hat{Z}_{uv}(j\omega_\ell) + \hat{Z}_{uv}^H(j\omega_\ell)\right]\sigma_\ell^2$$

which is positive-semidefinite by Assumption 1e. Define

$$\bar{G}_{uq}(z) \triangleq \left[I - \epsilon\bar{H}_{uq}(z^{-1})\right]\left[I + \epsilon\bar{H}_{uq}(z^{-1})\right]^{-1}$$

where $0 < \epsilon < \|\bar{H}_{uq}\|_{\mathbb{H}_\infty}^{-1}$. We then have that (24) holds if and only if $\|\bar{G}_{uq}(z)\| \leqslant 1$ for all $z \in \mathbb{C}_{\leqslant 1}$. Because $\bar{H}_{uq}(z)$ is analytic on $\mathbb{C}_{>1}$, it follows that $\bar{H}_{uq}(z^{-1})$ is analytic on $\mathbb{C}_{<1}$. But if $\bar{H}_{uq}(z^{-1})$ is analytic on $\mathbb{C}_{<1}$ then so is $\bar{G}_{uq}(z)$, and therefore via the Maximum Modulus Theorem, $\|\bar{G}_{uq}(z)\|$ attains is maximum on the boundary of $\mathbb{C}_{\leqslant 1}$, i.e., for $z = e^{j\Omega}$, $\Omega \in [-\pi, \pi]$. Because $\bar{H}_{uq}(e^{j\Omega}) + \bar{H}_{uq}(e^{-j\Omega}) \geqslant 0$, it follows that $\sup_{\Omega\in[-\pi,\pi]} \|\bar{G}_{uq}(e^{j\Omega})\| \leqslant 1$. This proves (24).

To prove the last caveat in claim (b), first consider the case where $|z| = 1$, i.e., $z = e^{j\Omega}$ for $\Omega \in [-\pi, \pi]$. Due to Assumption 1e, evaluation of $\bar{H}_{uq}(e^{j\Omega})$ as in (20) gives that inequality (24) must hold strictly unless $\mathrm{sn}(\omega_\ell T/2) = 0$ for all $\ell \in \mathbb{Z} \setminus \{0\}$. This only occurs if $\Omega = 0$, i.e., $z = 1$. Now, consider the case in which $z \in \mathbb{C}_{>0}$. Let $\nu \in \mathbb{C}^{n_p}$ and define $\bar{h}(z) \triangleq \nu^H\bar{H}_{uq}(z)\nu$. Consider the situation in which there exists a $z_0 \in \mathbb{C}_{>1}$ such that $\mathrm{Re}\left\{\bar{h}(z_0)\right\} = 0$, and define analytic function $\bar{g}(z) \triangleq \bar{h}(z) - j\mathrm{Im}\{\bar{h}(z_0)\}$. Then $\bar{g}(z_0) = 0$. Suppose it is the case that $\bar{g}(z) \neq 0$ for almost all z in an infinitesimal neighborhood of $z = z_0$. Let $z = z_0(1 + \delta e^{j\theta})$ where $\delta \in \mathbb{R}_{>0}$ is infinitesimal and $\theta \in [-\pi, \pi]$. Because $\bar{g}(z)$ is analytic at $z = z_0$, and δ is infinitesimal,

$$\bar{g}(z) = (z - z_0)^m\,\psi(z_0) = (z_0^m\delta^m\psi(z_0))\,e^{jm\theta}$$

where $\psi(z_0) = \lim_{z\to z_0} \bar{g}(z)(z - z_0)^{-m}$ and $m \in \mathbb{Z}_{>0}$ is the lowest integer such that $\psi(z_0) \neq 0$. It has been proven that $\mathrm{Re}\{\bar{g}(z)\} = \mathrm{Re}\{\bar{h}(z)\} \geqslant 0$ for all $z \in \mathbb{C}_{>1}$ and therefore we require that

$$z_0^m\psi(z_0)e^{jm\theta} + z_0^{mH}\psi^H(z_0)e^{-jm\theta} \geqslant 0, \quad \forall\theta \in [-\pi, \pi]. \quad (84)$$

Because $z_0\psi(z_0) \neq 0$, this is impossible. We therefore conclude that if $\bar{g}(z_0) = 0$ for some $z_0 \in \mathbb{C}_{>1}$ then it must be the case that $\bar{g}(z) = 0$ in some open neighborhood of $z = z_0$. But in order for $\bar{g}(z)$ to be analytic, this implies that $\bar{g}(z) = 0$ for all $z \in \mathbb{C}_{>1}$. If this is true then $\bar{g}(z) = 0$ almost everywhere on the boundary of $\mathbb{C}_{>1}$, i.e., for $z = e^{j\Omega}$ with $\Omega \in [-\pi, \pi]$. This in turn implies that $\mathrm{Re}\{\bar{h}(e^{j\Omega})\} = 0$ for almost all $\Omega \in [-\pi, \pi]$, which contradicts the last caveat in assumption 1e. We therefore conclude that $\mathrm{Re}\{\bar{h}(z)\} > 0$ everywhere in $\mathbb{C}_{>1}$. This holds for all $\nu \in \mathbb{C}^{n_p} \setminus \{0\}$, implying that $\bar{H}_{uq}(z) + \bar{H}_{uq}^H(z)$ is nonsingular over the same domain.

The first part of claim (c) is immediate from (18), together with claim (a). For the second part of the claim, we make a similar argument as above, resulting in the requirement that (84) hold at $z_0 = 1$. However, since $z_0 = 1$ is on the boundary of $\mathbb{C}_{\geqslant 1}$, rather than in the interior, it is only necessary that condition (84) hold for $\theta \in [-\frac{\pi}{2}, \frac{\pi}{2}]$. Satisfaction of the condition requires $m = 1$ and $z_0\gamma(z_0) \in \mathbb{R}_{>0}$. This proves that $\nu^H\left(\bar{H}_{ud}(1) + \bar{H}_{ud}^H(1)\right)\nu \in \mathbb{R}_{>0}$. Enforcing this for all $\nu \in \mathbb{C}^{n_p}$ implies that $\bar{H}_{ud}(1) + \bar{H}_{ud}^H(1) > 0$.

B. Proof of Theorem 2

To prove claim (a), it is known from Theorem 1 that $\left\{\bar{H}_{ud}, \bar{H}_{wa}, \bar{H}_{wd}\right\} \subset \mathbb{H}_\infty$. Meanwhile, the mapping $\boldsymbol{u} \mapsto \boldsymbol{a}$ is zero. As such, mapping $\{\boldsymbol{u}, \boldsymbol{w}\} \mapsto \{\boldsymbol{d}, \boldsymbol{a}\}$ is in $\mathbb{H}_\infty$. Minimality of realization (25) then implies that A is Schur.

To prove claim (b), it is a standard fact that $D_{uq} = \frac{1}{2\pi}\int_{-\pi}^{\pi} \bar{H}_{uq}(e^{j\Omega})d\Omega$ and consequently

$$\frac{1}{2\pi}\int_{-\pi}^{\pi} \left[\bar{H}_{uq}(e^{j\Omega}) + \bar{H}_{uq}^H(e^{j\Omega})\right]d\Omega = D_{uq} + D_{uq}^T$$

The integrand is positive-definite for almost all $\Omega \in [-\pi, \pi]$ so the integral is positive-definite.

To prove claim (c), we note that because $\bar{H}_{uq}(z)$ is PR and A is Schur, it follows that the transfer function $\bar{H}'_{uq}(z) \triangleq \bar{H}_{uq}(z) + \frac{1}{2}R$ is strongly strictly positive real, i.e., there exists a $\rho \in \mathbb{R}_{<1}$ such that $\bar{H}'_{uq}(\rho z) + \left[\bar{H}'_{uq}(\rho z)\right]^H > 0$ for all $z \in \mathbb{C}_{\geqslant 1}$. Claim (c) then follows directly from the generalized Kalman-Yakubovic-Popov Lemma. For continuous-time systems, this is shown in [60] (Section 3.12). The discrete-time case is directly analogous, and is omitted here for brevity.

C. Proof of Theorem 3

The matrix

$$A' \triangleq \begin{bmatrix} I & 0 \\ B_u^\perp AB_u[C_dB_u]^{-1} & A_s \end{bmatrix}$$

is similar to the matrix $A - B_uD_{uq}^{-1}C_q$. If η is an eigenvector of A_s, then $[0\ \eta^H]^H$ is an eigenvector of A'. Likewise, the eigenvalues of A' are those of A_s, together with $\lambda = 1$. We conclude that if the eigenvalues of $A - B_uD_{uq}^{-1}C_q$ are all in $\mathbb{C}_{<1} \cup \{1\}$, then these same properties hold for A_s.

Without loss of generality, we partition the state space to isolate the subspace controllable from u, i.e., we presume

$$A = \begin{bmatrix} A_{11} & A_{12} \\ 0 & A_{22} \end{bmatrix}, \qquad B_u = \begin{bmatrix} B_1 \\ 0 \end{bmatrix}, \qquad C_q = \begin{bmatrix} C_1^T \\ C_2^T \end{bmatrix}^T$$

and we have that

$$A - B_uD_{uq}^{-1}C_q = \begin{bmatrix} \Theta & A_{12} - B_1D_{uq}^{-1}C_2 \\ 0 & A_{22} \end{bmatrix}$$

where $\Theta \triangleq A_{11} - B_1D_{uq}^{-1}C_1$. It is known that the eigenvalues of $A - B_uD_{uq}^{-1}C_q$ are those of Θ and A_{22}. Furthermore, the eigenvalues of A_{22} have moduli strictly less than 1 because

A is Schur. So it follows that if λ is an eigenvalue of $A - B_u D_{uq}^{-1} C_q$ with $|\lambda| \geqslant 1$ then it is also an eigenvalue of Θ.

Now consider that

$$\bar{H}_{uq}^{-1} \sim \left[\begin{array}{c|c} \Theta & B_1 D_{uq}^{-1} \\ \hline -D_{uq}^{-1} C_1 & D_{uq}^{-1} \end{array}\right]$$

where we note that the above realization is minimal. Consequently, $\lambda \in \mathbb{C}$ is a pole of $\bar{H}_{uq}^{-1}(z)$ if and only if it is an eigenvalue of Θ. Because $\bar{H}_{uq}(z) + \bar{H}_{uq}^H(z) > 0$ for all $z \in \mathbb{C}_{\geqslant 1} \setminus \{1\}$, it follows that $\bar{H}_{uq}(z)$ is nonsingular in this domain, and consequently $\bar{H}_{uq}^{-1}(z)$ cannot have poles there. We conclude that all eigenvalues of A_s lie in $\mathbb{C}_{<1} \cup \{1\}$.

Assume $\lambda = 1$ is an eigenvalue of A_s. Then there exists a vector η such that

$$0 = \eta^H [A_s - I] = \eta^H B_u^\perp [A - I] C_d^\perp [B_u^\perp C_d^\perp]^{-1}$$

implying that there exists a vector ν such that

$$\eta^H B_u^\perp [A - I] = \nu^H C_d.$$

Because A is known to be Schur, $A - I$ is nonsingular and ν must be nonzero. Multiplying from the right by $[A - I]^{-1} B_u$ gives that $\nu^H \bar{H}_{ud}(1) = 0$, implying that $\lambda = 1$ is a zero of scalar transfer function $\nu^H \bar{H}_{ud}(z)\nu$. But $\bar{H}_{uq}(z) = \frac{1}{T}(z - 1)\bar{H}_{ud}(z)$ so $\lambda = 1$ must also be a zero of scalar transfer function $\nu^H \bar{H}_{uq}(z)\nu$. If $\nu^H \bar{H}_{ud}(z)\nu$ has a zero at $z = 1$, then $\nu^H \bar{H}_{uq}(z)\nu$ must have a repeated zero at $z = 1$. But because $\bar{H}_{uq}(z)$ is PR, it follows that $\nu^H \bar{H}_{uq}(z)\nu$ is positive-real, precluding the possibility of a repeated zero at $z = 1$. We conclude that $\lambda = 1$ cannot be an eigenvalue of A_s.

D. Proof of Theorem 4

We have that for some time $k \in \mathbb{Z}$,

$$\mathcal{E}\{\boldsymbol{p}_k\} = -\mathcal{E}\left\{\boldsymbol{u}_k^T C_q \boldsymbol{x}_k + \|\boldsymbol{u}_k\|_{\tilde{R}}^2 + v_d^T |\boldsymbol{u}_k|\right\}$$

where we recall that $\tilde{R} = \tilde{R}^T > 0$. It is straight-forward to verify that

$$\begin{aligned}\mathcal{E}\left\{\|\boldsymbol{u}_k\|_{\tilde{R}}^2\right\} =& \mathcal{E}\left\{\|\boldsymbol{\xi}_k\|_M^2\right\} + \mathcal{E}\left\{\|A\boldsymbol{x}_k + B_u\boldsymbol{u}_k\|_W^2\right\} \\ &- \mathcal{E}\left\{\|\boldsymbol{x}_k\|_W^2\right\} - \mathcal{E}\left\{\boldsymbol{u}_k^T C_q \boldsymbol{x}_k\right\}\end{aligned}$$

Because $\boldsymbol{x}_k$ and $\boldsymbol{u}_k$ are independent of $\boldsymbol{w}_k$, and because $\boldsymbol{w}_k$ is zero-mean with $\mathcal{E}\{\boldsymbol{w}_k \boldsymbol{w}_k^T\} = S_w$,

$$\begin{aligned}\mathcal{E}\left\{\|\boldsymbol{u}_k\|_{\tilde{R}}^2\right\} =& \mathcal{E}\left\{\|\boldsymbol{\xi}_k\|_M^2\right\} - \mathcal{E}\left\{\boldsymbol{u}_k^T C_q \boldsymbol{x}_k\right\} - \bar{p} \\ &+ \mathcal{E}\left\{\|\boldsymbol{x}_{k+1}\|_W^2\right\} - \mathcal{E}\left\{\|\boldsymbol{x}_k\|_W^2\right\}.\end{aligned}$$

Summing over $k \in \{0, ..., \tau\}$ and dividing by $\tau + 1$ gives the claimed result, if (53) holds.

E. Proof of Lemma 1

Substitute (69), (70), and (71) into (72), with $J(\cdot, \cdot, \cdot)$ defined as in (56), to get

$$\begin{aligned}&\rho(x_{k+h+1|k}) \\ &= x_{k+h+1|k}^T \left(\sum_{i=0}^{\infty} Q_i\right) x_{k+h+1|k} + v_d^T \left(\sum_{i=0}^{\infty} \left|u_{k+h+1+i|k}\right|\right) \\ &\quad + \mu \left(\sum_{i=0}^{\infty} u_{\max}^T \max\left\{0, \left|u_{k+h+1+i|k}\right| - u_{\max}\right\}\right) \qquad (85)\end{aligned}$$

where, for $i \in \mathbb{Z}_{\geqslant 0}$,

$$\begin{aligned}Q_i \triangleq& (B_u^\perp)^T (A_s^i)^T C_s^T (F + D_{uq}^{-1} C_q)^T \\ &\times M (F + D_{uq}^{-1} C_q) C_s A_s^i B_u^\perp\end{aligned}$$

By Theorem 3, A_s is Schur, and so $\sum_{i=0}^{\infty} Q_i = (B_u^\perp)^T Z B_u^\perp$ where $Z = Z^T \geqslant 0$ is the unique solution to discrete-time Lyapunov equation

$$Z = A_s^T Z A_s + C_s^T (F + D_{uq}^{-1} C_q)^T M (F + D_{uq}^{-1} C_q) C_s$$

There is no convenient closed-form solution for the second summation in (85), so we seek to over-bound it by a simple function of $x_{k+h+1|k}$. To do this, first let $\Pi \in \mathbb{C}^{n \times n}$ be a similarity transformation that converts A_s to its Jordan form Λ, i.e., $A_s = \Pi \Lambda \Pi^{-1}$. Then we have that

$$\begin{aligned}\left|u_{k+h+1+i|k}\right| =& \sum_{i=0}^{\infty} \left|D_{uq}^{-1} C_q C_s \Pi \ \Lambda^i \ \Pi^{-1} \ B_u^\perp x_{k+h+1|k}\right| \\ \leqslant& \sum_{i=0}^{\infty} \left|D_{uq}^{-1} C_q C_s \Pi\right| \ |\Lambda|^i \ \left|\Pi^{-1} B_u^\perp x_{k+h+1|k}\right| \\ =& \left|D_{uq}^{-1} C_q C_s \Pi\right| [I - |\Lambda|]^{-1} \left|\Pi^{-1} B_u^\perp x_{k+h+1|k}\right|\end{aligned}$$

where we note that the above infinite summation converges because if Λ is a Schur Jordan form, then so is $|\Lambda|$.

The last term in (85) can be conservatively over-bounded by first recognizing that

$$u_{\max}^T \max\{0, |u_{k+h+1+i|k}| - u_{\max}\} \leqslant \tfrac{1}{4} \|u_{k+h+1+i|k}\|_2^2 \qquad (86)$$

But

$$\sum_{i=0}^{\infty} \|u_{k+h+1+i|k}\|^2 = x_{k+h+1|k}^T (B_u^\perp)^T X B_u^\perp x_{k+h+1|k}$$

where $X = X^T \geqslant 0$ is the solution to Lyapunov equation

$$X = A_s^T X A_s + C_s^T C_q^T D_{uq}^{-T} D_{uq}^{-1} C_q C_s.$$

We arrive at an over-bound for $\rho(x_{k+h+1|k})$ as in (74), with

$$\begin{aligned}Q_f =& (B_u^\perp)^T (Z + \tfrac{1}{4}\mu X) B_u^\perp \\ C_f =& \operatorname{diag}\left\{[I - |\Lambda|]^{-T} \left|D_{uq}^{-1} C_q C_s \Pi\right|^T v_d\right\} \Pi^T B_u^\perp\end{aligned}$$

To prove inequality (75), consider that because $x_{k+h+2|k} = C_s A_s B_u^\perp x_{k+h+1|k}$ and $B_u^\perp C_s = I$, we have that

$$J_f(x_{k+h+2|k}) = \left\|B_u^\perp x_{k+h+1|k}\right\|_\Xi^2 + \|C_f x_{k+h+1|k}\|_1$$

where

$$\begin{aligned}\Xi \triangleq& A_s^T (Z + \tfrac{1}{4}\mu X) A_s \\ =& (Z + \tfrac{1}{4}\mu X) - C_s^T (F + D_{uq}^{-1} C_q)^T M (F + D_{uq}^{-1} C_q) C_s \\ &- \tfrac{1}{4}\mu C_s^T C_q^T D_{uq}^T D_{uq}^{-1} C_q C_s\end{aligned}$$

and therefore

$$\begin{aligned}\left\|B_u^\perp x_{k+h+1|k}\right\|_\Xi^2 =& \left\|x_{k+h+1|k}\right\|_{Q_f}^2 - \tfrac{1}{4}\mu \left\|u_{k+h+1|k}\right\|^2 \\ &- \left\|u_{k+h+1|k} - F x_{k+h+1|k}\right\|_M^2\end{aligned}$$

Also, consider that

$$\begin{aligned}
&\|C_f x_{k+h+2|k}\|_1 \\
&= v_d^T \left|D_{uq}^{-1} C_q C_s \Pi\right| \left[I - |\Lambda|\right]^{-1} \left|\Pi^{-1} B_u^{\perp} x_{k+h+2|k}\right| \\
&= v_d^T \left|D_{uq}^{-1} C_q C_s \Pi\right| \left[I - |\Lambda|\right]^{-1} \left|\Pi^{-1} A_s B_u^{\perp} x_{k+h+1|k}\right| \\
&= v_d^T \left|D_{uq}^{-1} C_q C_s \Pi\right| \left[I - |\Lambda|\right]^{-1} \left|\Lambda \Pi^{-1} B_u^{\perp} x_{k+h+1|k}\right| \\
&\leqslant v_d^T \left|D_{uq}^{-1} C_q C_s \Pi\right| \left[I - |\Lambda|\right]^{-1} |\Lambda| \left|\Pi^{-1} B_u^{\perp} x_{k+h+1|k}\right| \\
&= \|C_f x_{k+h+1|k}\|_1 \\
&\quad - v_d^T \left|D_{uq}^{-1} C_q C_s \Pi\right| \left|\Pi^{-1} B_u^{\perp} x_{k+h+1|k}\right| \\
&\leqslant \|C_f x_{k+h+1|k}\|_1 - v_d^T \left|D_{uq}^{-1} C_q x_{k+h+1|k}\right| \\
&= \|C_f x_{k+h+1|k}\|_1 - v_d^T \left|u_{k+h+1|k}\right|
\end{aligned}$$

Recalling (86), we conclude (75).

F. Proof of Theorem 5

We begin with two technical lemmas which establish various bounds that will be useful in the sequel.

Lemma 2: Let $K : Y_k \mapsto u_k$ be as in (63). Then there exist constants $\{c_1, c_2\} \in \mathbb{R}_{>0}$ such that

$$\Gamma(x_k, \mathring{U}_{k|k}, \mathring{B}_{k|k}) \leqslant c_2 \|x_k\|_2^2 + c_1 \|x_k\|_1 \tag{87}$$

Proof: For a given x_k, let the (sub-optimal) sequence $U_{k|k}$ be the sequence rendering $d_{m|k} = 0$ for all $m > k$, i.e.,

$$u_{m|k} = \begin{cases} -\frac{1}{T} D_{uq}^{-1} C_d A x_k & : \quad m = k \\ -D_{uq}^{-1} C_q C_s A_s^{m-k} B_u^{\perp} x_k & : \quad m > k \end{cases}$$

and let corresponding sequence $B_{k|k}$ be the minimum value that satisfies the force constraint, i.e.,

$$b_{m|k} = \max\{0, |u_{m|k}| - u_{\max}\}.$$

Then the fact that $\{U_{k|k}, B_{k|k}\}$ are feasible for initial condition x_k implies that that $\Gamma(x_k, U_{k|k}, B_{k|k}) \geqslant \Gamma(x_k, \mathring{U}_{k|k}, \mathring{B}_{k|k})$. Furthermore, by repeated application of Lemma 1 that

$$\begin{aligned}
&\Gamma(x_k, U_{k|k}, B_{k|k}) \\
&\leqslant J_f(x_{k+1|k}) + J(x_k, u_{k|k}, b_{k|k}) \\
&= \|x_{k+1|k}\|_{Q_f}^2 + \|C_f x_{k+1|k}\|_1 + \|u_{k|k} - F x_{k|k}\|_M^2 \\
&\quad + (v_d + \mu u_{\max})^T |u_{k|k}|
\end{aligned}$$

where we have used the fact that $b_{k|k} \leqslant |u_{k|k}|$. Substitution of the expression above for $u_{k|k}$, and using the fact that $C_s B_u^{\perp} = I$, we have that

$$\begin{aligned}
&\Gamma(x_k, U_{k|k}, B_{k|k}) \leqslant \|\check{A} x_k\|_{Q_f}^2 + \|C_f \check{A} x_k\|_1 \\
&\quad + \|(F + \tfrac{1}{T} D_{uq}^{-1} C_d) x_k\|_M^2 + (v_d + \mu u_{\max})^T |\tfrac{1}{T} D_{uq}^{-1} C_d x_k|
\end{aligned}$$

where $\check{A} \triangleq (I - \frac{1}{T} B_u D_{uq}^{-1} C_d) A$. It is then straight-forward to show by defining c_1 and c_2 as

$$\begin{aligned}
c_1 &= \|C_f \check{A}\|_1 + \left\|\mathrm{diag}\{v_d + \mu u_{\max}\} \tfrac{1}{T} D_{uq}^{-1} C_d\right\|_1 \\
c_2 &= \|Q_f^{1/2} \check{A}\|_2^2 + \|M^{1/2}(F + \tfrac{1}{T} D_{uq}^{-1} C_d)\|_2^2
\end{aligned}$$

we have that

$$\Gamma(x_k, U_{k|k}, B_{k|k}) \leqslant c_2 \|x_k\|_2^2 + c_1 \|x_k\|_1.$$

Recalling that $\Gamma(x_k, U_{k|k}, B_{k|k}) \geqslant \Gamma(x_k, \mathring{U}_{k|k}, \mathring{B}_{k|k})$ completes the proof. ∎

Lemma 3: For x_k^i, $i \in \{1, 2\}$, let $U_{k|k}^i$ and $B_{k|k}^i$ satisfy

$$\Theta(x_k^i, U_{k|k}^i, B_{k|k}^i) \leqslant 0, \qquad \Psi(x_k^i, U_{k|k}^i) = 0 \tag{88}$$

Let the corresponding receding-horizon trajectories with these input sequences be $x_{m|k}^i$ for $m \geqslant k$. Define perturbations $\tilde{U}_{k|k} = U_{k|k}^2 - U_{k|k}^1$ and $\tilde{B}_{k|k} = B_{k|k}^2 - B_{k|k}^1$, and $\tilde{x}_{m|k} = x_{m|k}^2 - x_{m|k}^1$. Then

$$\begin{aligned}
&\Gamma(x_k^2, U_{k|k}^2, B_{k|k}^2) \leqslant \Gamma(x_k^1, U_{k|k}^1, B_{k|k}^1) \\
&\quad + 2\Gamma^{1/2}(x_k^1, U_{k|k}^1, B_{k|k}^1) \chi_k^{1/2} + \Gamma(\tilde{x}_k, \tilde{U}_{k|k}, |\tilde{B}_{k|k}|)
\end{aligned} \tag{89}$$

where

$$\chi_k \triangleq \sum_{m=k}^{k+h} \|\tilde{u}_{m|k} - F \tilde{x}_{m|k}\|_M^2 + \|\tilde{x}_{k+h+1|k}\|_{Q_f}^2 \tag{90}$$

Proof: We have that

$$\begin{aligned}
&\Gamma(x_k^2, U_{k|k}^2, B_{k|k}^2) \\
&= \sum_{m=k}^{k+h} \left\|u_{m|k}^1 - F x_{m|k}^1\right\|_M^2 + \sum_{m=k}^{k+h} \left\|\tilde{u}_{m|k} - F \tilde{x}_{m|k}\right\|_M^2 \\
&\quad + 2 \sum_{m=k}^{k+h} \left(u_{m|k}^1 - F x_{m|k}^1\right)^T M \left(\tilde{u}_{m|k} - F \tilde{x}_{m|k}\right) \\
&\quad + \sum_{m=k}^{k+h} \left(v_d^T \left|u_{m|k}^1 + \tilde{u}_{m|k}\right| + \mu u_{\max}^T (b_{m|k}^1 + \tilde{b}_{m|k})\right) \\
&\quad + \|x_{k+h+1}^1\|_{Q_f}^2 + \|\tilde{x}_{k+h+1}\|_{Q_f}^2 + 2 \tilde{x}_{k+h+1}^T Q_f x_{k+h+1}^1 \\
&\quad + \|C_f x_{k+h+1} + C_f \tilde{x}_{k+h+1}\|_1
\end{aligned}$$

Via the Cauchy-Schwartz inequality,

$$\begin{aligned}
&\sum_{m=k}^{k+h} \left(u_{m|k}^1 - F x_{m|k}^1\right)^T M \left(\tilde{u}_{m|k} - F \tilde{x}_{m|k}\right) \\
&\quad + \tilde{x}_{k+h+1}^T Q_f x_{k+h+1}^1 \\
&\leqslant \left(\sum_{m=k}^{k+h} \left\|u_{m|k}^1 - F x_{m|k}^1\right\|_M^2 + \|x_{k+h+1}^1\|_{Q_f}^2\right)^{1/2} \chi_k \\
&\leqslant \Gamma^{1/2}(x_k^1, U_{k|k}^1, B_{k|k}^1) \chi_k
\end{aligned}$$

and via the triangle inequality,

$$\begin{aligned}
&\sum_{m=k}^{k+h} v_d^T \left|u_{m|k}^1 + \tilde{u}_{m|k}\right| + \left\|C_f x_{k+h+1}^1 + C_f \tilde{x}_{k+h+1}\right\|_1 \\
&\leqslant \sum_{m=k}^{k+h} v_d^T \left|u_{m|k}^1\right| + \sum_{m=k}^{k+h} v_d^T \left|\tilde{u}_{m|k}\right| \\
&\quad + \left\|C_f x_{k+h+1}^1\right\|_1 + \|C_f \tilde{x}_{k+h+1}\|_1
\end{aligned}$$

Also, note that because $b_{m|k}^1$ and $b_{m|k}^2$ are both nonnegative,

$$u_{\max}^T (b_{m|k}^1 + \tilde{b}_{m|k}) \leqslant u_{\max}^T b_{m|k}^1 + u_{\max}^T |\tilde{b}_{m|k}|.$$

Substituting these inequalities gives (89). ∎

Let the present time be k, and let $\mathring{U}_{k|k}$ and $\mathring{B}_{k|k}$ be the trajectories found by the MPC algorithm (63), given present state x_k. For $m \geqslant k$, let the optimized receding-horizon state trajectory be denoted $\mathring{x}_{m|k}$, with $\mathring{x}_{k|k} = x_k$. Let $\mathring{d}_{m|k}$ be as in (67), evaluated with the optimal trajectories, i.e., $\mathring{d}_{m|k} =$

$C_d\mathring{x}_{m|k}$, where we note that $\mathring{d}_{k+h+1|k}=0$. For $m>k+h$, let $\mathring{u}_{m|k}$ be the post-horizon input that enforces $\mathring{d}_{m|k}=0$, i.e.,

$$\begin{aligned}\mathring{x}_{m|k} =&C_sA_s^{m-(k+h+1)}B_u^{\perp}\mathring{x}_{k+h+1|k}\\ \mathring{u}_{m|k} =&-D_{uq}^{-1}C_q\mathring{x}_{m|k}\end{aligned}$$

Now, we advance the present time to $k+1$. With acquisition of data y_k, the data w_k and x_{k+1} become known. We consider the receding-horizon control trajectory $U_{k+1|k+1}$ that enforces

$$d_{m|k+1}=\mathring{d}_{m|k},\quad \forall m\in\{k+2,...,k+h+2\}. \tag{91}$$

Corresponding slack variable sequence $B_{k+1|k+1}$ has components

$$b_{m|k+1}=\max\left\{0,|u_{m|k+1}|-u_{\max}\right\}$$

Note that, so formulated, this trajectory pair $\{U_{k+1|k+1},B_{k+1|k+1}\}$ satisfies the constraints in the MPC algorithm at the $(k+1)^{th}$ iteration, i.e., conditions

$$\Theta(x_{k+1},U_{k+1|k+1},B_{k+1|k+1})\leqslant 0,\quad \Psi(x_{k+1},U_{k+1|k+1})=0$$

and is therefore in the feasibility domain for the MPC optimization algorithm at time $k+1$.

We now claim that the sequence $U_{k+1|k+1}$ resulting in (91), and the associated receding-horizon sequence $\{x_{m|k+1}:m\geqslant k+1\}$, can be expressed as

$$u_{m|k+1}=\mathring{u}_{m|k}+\tilde{u}_{m|k+1},\qquad x_{m|k+1}=\mathring{x}_{m|k}+\tilde{x}_{m|k+1}$$

where

$$\tilde{u}_{m|k+1}=-\tfrac{1}{T}D_{uq}^{-1}C_dA\tilde{x}_{m|k+1} \tag{92}$$

$$\tilde{x}_{m|k+1}=\begin{cases}B_ww_k & :\quad m=k+1\\ \tilde{A}^{m-k-1}B_ww_k & :\quad m>k+1\end{cases} \tag{93}$$

with $\tilde{A}\triangleq C_d^{\perp}[B_u^{\perp}C_d^{\perp}]^{-1}B_u^{\perp}A$. To show this, consider the inverse system dynamic model from Section II-D. Let

$$\zeta_{m|k+1}\triangleq\mathcal{E}\{\boldsymbol{\zeta}_m|\boldsymbol{Y}_{k+1}=Y_{k+1},\ \boldsymbol{d}_m=d_{m|k+1},\forall m\geqslant k+1\}.$$

Then we have that for $m\geqslant k+1$,

$$\zeta_{m+1|k+1}=A_s\zeta_{m|k+1}+B_{ds}d_{m|k+1}$$

with initial condition

$$\zeta_{k+1|k+1}=A_s\zeta_k+B_{ws}w_k+B_{ds}d_k$$

But we also have that for $m\geqslant k+1$,

$$\mathring{\zeta}_{m+1|k}=A_s\mathring{\zeta}_{m|k}+B_{ds}\mathring{d}_{m|k}$$

with initial condition

$$\mathring{\zeta}_{k+1|k}=A_s\zeta_k+B_{ds}\mathring{d}_{k|k}$$

So, letting $\tilde{\zeta}_{m|k+1}\triangleq\zeta_{m|k+1}-\mathring{\zeta}_{m|k}$, we have that

$$\tilde{\zeta}_{m+1|k+1}=A_s\tilde{\zeta}_{m|k+1}+B_{ds}\left(d_{m|k+1}-\mathring{d}_{m|k}\right)$$

with initial condition

$$\tilde{\zeta}_{k+1|k+1}=B_{ws}w_k+B_{ds}\left(d_k-\mathring{d}_{k|k}\right)$$

But $d_k-\mathring{d}_{k|k}=D_{wd}w_k$, so using (45), the above initial condition simplifies to $\tilde{\zeta}_{k+1|k+1}=B_u^{\perp}B_ww_k$. Also, we have that $d_{k+1|k+1}-\mathring{d}_{k+1|k}=C_dB_ww_k$ while for $m>k+1$, (91) implies that $d_{m|k+1}-\mathring{d}_{m|k}=0$. Consequently, we have that for $m>k+1$,

$$\begin{aligned}\tilde{\zeta}_{m|k+1}=&A_s^{m-k-2}\left[A_sB_u^{\perp}+B_{ds}C_d\right]B_ww_k\\ =&A_s^{m-k-2}B_u^{\perp}AB_ww_k\end{aligned}$$

where we have used (44) and (45) in the second line. For $m\geqslant k+1$, it follows from (43) and the above, that

$$\tilde{x}_{m|k+1}=\begin{cases}C_sB_u^{\perp}B_ww_k+D_{ds}C_dB_ww_k & :\quad m=k+1\\ C_sA_s^{m-k-2}B_u^{\perp}AB_ww_k & :\quad m>k+1\end{cases}$$

which simplifies to (93). Using (38), this implies that

$$\tilde{u}_{m|k+1}=-D_{uq}^{-1}C_q\tilde{x}_{m|k+1}+\tfrac{1}{T}D_{uq}^{-1}\left(\tilde{d}_{m+1|k+1}-\tilde{d}_{m|k+1}\right).$$

Use of (93) and (44)-(47) give the above as equivalent to (92).

Define sequences $\mathring{U}_{k+1|k}=\{\mathring{u}_{k+1|k},...,\mathring{u}_{k+h+1|k}\}$ and $\mathring{B}_{k+1|k}=\{\mathring{b}_{k+1|k},...,\mathring{b}_{k+h+1|k}\}$. Then we have that the pair $\{\mathring{U}_{k+1|k},\mathring{B}_{k+1|k}\}$ are in the feasibility domain of MPC optimization algorithm (63) at time $k+1$ given initial condition $\mathring{x}_{k+1|k}$. From Lemma 3, we infer that

$$\begin{aligned}\Gamma(x_{k+1},U_{k+1|k+1},B_{k+1|k+1})\leqslant&\,\Gamma(\mathring{x}_{k+1|k},\mathring{U}_{k+1|k},\mathring{B}_{k+1|k})\\ &+2\Gamma^{1/2}(\mathring{x}_{k+1|k},\mathring{U}_{k+1|k},\mathring{B}_{k+1|k})\chi_{k+1}\\ &+\Gamma(\tilde{x}_{k+1},\tilde{U}_{k+1|k+1},|\tilde{U}_{k+1|k+1}|)\end{aligned}$$

where

$$\chi_{k+1}\triangleq\sum_{m=k+1}^{k+h+1}\|\tilde{u}_{m|k+1}-F\tilde{x}_{m|k+1}\|_M^2+\|\tilde{x}_{k+h+2|k+1}\|_{Q_f}^2 \tag{94}$$

From Lemma 1 we have inequality (75), and therefore

$$\Gamma(x_k,\mathring{U}_{k|k},\mathring{B}_{k|k})\geqslant J(x_k,u_k,b_k)+\Gamma(\mathring{x}_{k+1|k},\mathring{U}_{k+1|k},\mathring{B}_{k+1|k}).$$

So it follows that

$$\begin{aligned}\Gamma(x_{k+1},U_{k+1|k+1},B_{k+1|k+1})\leqslant&\,\Gamma(x_k,\mathring{U}_{k|k},\mathring{B}_{k|k})\\ &-J(x_k,u_k,b_k)+2\Gamma^{1/2}(\mathring{x}_{k+1|k},\mathring{U}_{k+1|k},\mathring{B}_{k+1|k})\chi_{k+1}\\ &+\Gamma(\tilde{x}_k,\tilde{U}_{k|k},|\tilde{U}_{k|k}|)\end{aligned}$$

Now, using Lemma 2, we note that

$$\begin{aligned}&\Gamma^{1/2}(\mathring{x}_{k+1|k},\mathring{U}_{k+1|k},\mathring{B}_{k+1|k})\\ &\leqslant\left[\Gamma(\mathring{x}_{k|k},\mathring{U}_{k|k},\mathring{B}_{k|k})-J(x_k,u_k,b_k)\right]^{1/2}\\ &\leqslant\Gamma^{1/2}(\mathring{x}_{k|k},\mathring{U}_{k|k},\mathring{B}_{k|k})\\ &\leqslant\left[c_2\|x_k\|_2^2+c_1\|x_k\|_1\right]^{1/2}\\ &\leqslant\left[c_2\|x_k\|_2^2+c_1\sqrt{n}\|x_k\|_2\right]^{1/2}\\ &\leqslant\sqrt{c_2}\left[\|x_k\|_2+\frac{c_1\sqrt{n}}{2c_2}\right]\end{aligned}$$

So we conclude that

$$\begin{aligned}\Gamma(x_{k+1},U_{k+1|k+1},B_{k+1|k+1})\leqslant&\,\Gamma(x_k,\mathring{U}_{k|k},\mathring{B}_{k|k})\\ &-J(x_k,u_k,b_k)+2\sqrt{c_2}\left[\|x_k\|_2+\frac{c_1\sqrt{n}}{2c_2}\right]\chi_{k+1}\\ &+\Gamma(\tilde{x}_k,\tilde{U}_{k|k},|\tilde{U}_{k|k}|)\end{aligned}$$

Due to (92) and (93), together with (65) and (94), it follows that there exist constants a_1, a_2, and a_3 such that

$$\chi_{k+1}^{1/2} \leqslant a_1\|w_k\|_2 \leqslant a_1\|w_k\|_1$$
$$\Gamma(\tilde{x}_k, \tilde{U}_{k|k}, |\tilde{U}|_{k|k}) \leqslant a_2\|w_k\|_2^2 + a_3\|w_k\|_1$$

As such, we conclude that

$$\begin{aligned} &J(x_k, u_k, b_k) \\ &\leqslant \Gamma(x_k, \mathring{U}_{k|k}, \mathring{B}_{k|k}) - \Gamma(x_{k+1}, U_{k+1|k+1}, B_{k+1|k+1}) \\ &\quad + a_2\|w_k\|_2^2 + a_4\|w_k\|_1 + a_5\|x_k\|_2\|w_k\|_2 \end{aligned}$$

where $a_4 \triangleq a_3 + a_1c_1\sqrt{n/c_2}$ and $a_5 \triangleq 2\sqrt{c_2}a_1$.

Now consider the implementation of MPC optimization algorithm (63) at time $k+1$, resulting in optimal sequences $\mathring{U}_{k+1|k+1}$ and $\mathring{B}_{k+1|k+1}$. Because sequences $U_{k+1|k+1}$ and $B_{k+1|k+1}$ derived above are feasible, it follows that

$$\begin{aligned} &\Gamma(x_{k+1}, \mathring{U}_{k+1|k+1}, \mathring{B}_{k+1|k+1}) \\ &\qquad \leqslant \Gamma(x_{k+1}, U_{k+1|k+1}, B_{k+1|k+1}) \end{aligned}$$

Define r_τ for all $\tau \in \mathbb{Z}_{\geqslant 0}$ as

$$r_\tau \triangleq \sum_{k=0}^{\tau} J(x_k, u_k, b_k)$$

Then the above inequalities imply that

$$\begin{aligned} r_\tau \leqslant &\Gamma(x_0, \mathring{U}_{0|0}, \mathring{B}_{0|0}) + a_2\|w\|_{2\tau}^2 + a_4\|w\|_{1\tau} \\ &+ a_5\sum_{k=0}^{\tau}\|x_k\|_2\|w_k\|_2 \end{aligned}$$

Using Lemma 2 and the Cauchy-Schwartz inequality,

$$\begin{aligned} r_\tau \leqslant &c_2\|x_0\|_2^2 + c_1\|x_0\|_1 + a_2\|w\|_{2\tau}^2 + a_4\|w\|_{1\tau} \\ &+ a_5\|x\|_{2\tau}\|w\|_{2\tau} \end{aligned}$$

Let $\delta_k \triangleq M^{1/2}(u_k - Fx_k)$. Then $r_\tau \geqslant \|\delta\|_{2\tau}^2$, and thus

$$\begin{aligned} \|\delta\|_{2\tau}^2 \leqslant &c_2\|x_0\|_2^2 + c_1\|x_0\|_1 + a_2\|w\|_{2\tau}^2 + a_4\|w\|_{1\tau} \\ &+ a_5\|x\|_{2\tau}\|w\|_{2\tau} \end{aligned}$$

Meanwhile, consider that

$$x_{k+1} = [A + B_uF]\,x_k + B_uM^{-1/2}\delta_k + B_ww_k$$

where we recall from Theorem 2 that $[A + B_uF]$ is Schur. It follows that there exist $\{\vartheta, \varphi\} \subset \mathbb{R}_{>0}$ such that

$$\|x\|_{2\tau}^2 \leqslant \vartheta\|\delta\|_{2\tau}^2 + \varphi\|w\|_{2\tau}^2$$

for all $\tau \in \mathbb{R}_{>0}$. So we conclude that

$$\begin{aligned} 0 \geqslant &\|x\|_{2\tau}^2 - \vartheta a_5\|w\|_{2\tau}\|x\|_{2\tau} \\ &- \left(\vartheta c_2\|x_0\|_2^2 + \vartheta c_1\|x_0\|_1 + (\vartheta a_2 + \varphi)\|w\|_{2\tau}^2 + \vartheta a_4\|w\|_{1\tau}\right) \end{aligned}$$

The right-hand side is convex in $\|x\|_{2\tau}$, with real roots. So

$$\begin{aligned} \|x\|_{2\tau} \leqslant &\tfrac{1}{2}\vartheta a_5\|w\|_{2\tau} \\ &+ \sqrt{\begin{array}{l}\vartheta c_2\|x_0\|_2^2 + \vartheta c_1\|x_0\|_1 + \vartheta a_4\|w\|_{1\tau} \\ +(\vartheta a_2 + \varphi + \frac{1}{4}\vartheta^2 a_5^2)\|w\|_{2\tau}^2\end{array}} \end{aligned}$$

Inequality (77) is obtained by squaring the above and then linearizing the (concave) square root about the value $\frac{1}{2}\vartheta a_5\|w\|_{2\tau}$.

REFERENCES

[1] M. E. McCormick, *Ocean wave energy conversion*. Courier Corporation, 2013.

[2] F. d. O. Antonio, "Wave energy utilization: A review of the technologies," *Renewable and sustainable energy reviews*, vol. 14, no. 3, pp. 899–918, 2010.

[3] D. Clemente, P. Rosa-Santos, and F. Taveira-Pinto, "On the potential synergies and applications of wave energy converters: A review," *Renewable and Sustainable Energy Reviews*, vol. 135, p. 110162, 2021.

[4] B. Guo and J. V. Ringwood, "A review of wave energy technology from a research and commercial perspective," *IET Renewable Power Generation*, vol. 15, no. 14, pp. 3065–3090, 2021.

[5] J. Falnes, "A review of wave-energy extraction," *Marine structures*, vol. 20, no. 4, pp. 185–201, 2007.

[6] S. H. Salter, J. Taylor, and N. Caldwell, "Power conversion mechanisms for wave energy," *Proceedings of the Institution of Mechanical Engineers, Part M: Journal of Engineering for the Maritime Environment*, vol. 216, no. 1, pp. 1–27, 2002.

[7] M. A. Jusoh, M. Z. Ibrahim, M. Z. Daud, A. Albani, and Z. Mohd Yusop, "Hydraulic power take-off concepts for wave energy conversion system: A review," *Energies*, vol. 12, no. 23, p. 4510, 2019.

[8] R. Ahamed, K. McKee, and I. Howard, "Advancements of wave energy converters based on power take off (pto) systems: A review," *Ocean Engineering*, vol. 204, p. 107248, 2020.

[9] ——, "A review of the linear generator type of wave energy converters? power take-off systems," *Sustainability*, vol. 14, no. 16, p. 9936, 2022.

[10] D. B. Murray, J. G. Hayes, D. L. O'Sullivan, and M. G. Egan, "Supercapacitor testing for power smoothing in a variable speed offshore wave energy converter," *IEEE Journal of Oceanic Engineering*, vol. 37, no. 2, pp. 301–308, 2012.

[11] E. Tedeschi and M. Santos-Mugica, "Modeling and control of a wave energy farm including energy storage for power quality enhancement: The bimep case study," *IEEE Transactions on Power Systems*, vol. 29, no. 3, pp. 1489–1497, 2013.

[12] J. Hals, J. Falnes, and T. Moan, "A comparison of selected strategies for adaptive control of wave energy converters," *Journal of Offshore Mechanics and Arctic Engineering*, vol. 133, no. 3, 2011.

[13] J. Scruggs, S. Lattanzio, A. Taflanidis, and I. Cassidy, "Optimal causal control of a wave energy converter in a random sea," *Applied Ocean Research*, vol. 42, pp. 1–15, 2013.

[14] J. V. Ringwood, G. Bacelli, and F. Fusco, "Energy-maximizing control of wave-energy converters: The development of control system technology to optimize their operation," *IEEE control systems magazine*, vol. 34, no. 5, pp. 30–55, 2014.

[15] R. G. Coe, G. Bacelli, D. G. Wilson, O. Abdelkhalik, U. A. Korde, and R. D. Robinett III, "A comparison of control strategies for wave energy converters," *International journal of marine energy*, vol. 20, pp. 45–63, 2017.

[16] J. Falnes, "Radiation impedance matrix and optimum power absorption for interacting oscillators in surface waves," *Applied ocean research*, vol. 2, no. 2, pp. 75–80, 1980.

[17] D. Evans, "Power from water waves," *Annual review of Fluid mechanics*, vol. 13, no. 1, pp. 157–187, 1981.

[18] P. Nebel, "Maximizing the efficiency of wave-energy plant using complex-conjugate control," *Proceedings of the Institution of Mechanical Engineers, Part I: Journal of Systems and Control Engineering*, vol. 206, no. 4, pp. 225–236, 1992.

[19] S. Zhan and G. Li, "Linear optimal noncausal control of wave energy converters," *IEEE Transactions on Control Systems Technology*, vol. 27, no. 4, pp. 1526–1536, 2018.

[20] D. Evans, "Maximum wave-power absorption under motion constraints," *Applied Ocean Research*, vol. 3, no. 4, pp. 200–203, 1981.

[21] J. Hals, J. Falnes, and T. Moan, "Constrained optimal control of a heaving buoy wave-energy converter," *Journal of Offshore Mechanics and Arctic Engineering*, vol. 133, no. 1, 2011.

[22] G. Bacelli and J. Ringwood, "Constrained control of arrays of wave energy devices," *International Journal of Marine Energy*, vol. 3, pp. e53–e69, 2013.

[23] M. Penalba, G. Giorgi, and J. V. Ringwood, "Mathematical modelling of wave energy converters: A review of nonlinear approaches," *Renewable and Sustainable Energy Reviews*, vol. 78, pp. 1188–1207, 2017.

[24] J. Cretel, A. Lewis, G. Lightbody, and G. Thomas, "An application of model predictive control to a wave energy point absorber," *IFAC Proceedings Volumes*, vol. 43, no. 1, pp. 267–272, 2010.

[25] M. Richter, M. E. Magana, O. Sawodny, and T. K. Brekken, "Nonlinear model predictive control of a point absorber wave energy converter," *IEEE Transactions on Sustainable Energy*, vol. 4, no. 1, pp. 118–126, 2012.

[26] G. Li and M. R. Belmont, "Model predictive control of sea wave energy converters–part i: A convex approach for the case of a single device," *Renewable Energy*, vol. 69, pp. 453–463, 2014.

[27] N. Tom and R. W. Yeung, "Experimental confirmation of nonlinear-model-predictive control applied offline to a permanent magnet linear generator for ocean-wave energy conversion," *IEEE Journal of Oceanic Engineering*, vol. 41, no. 2, pp. 281–295, 2015.

[28] N. Faedo, S. Olaya, and J. V. Ringwood, "Optimal control, mpc and mpc-like algorithms for wave energy systems: An overview," *IFAC Journal of Systems and Control*, vol. 1, pp. 37–56, 2017.

[29] Q. Zhong and R. W. Yeung, "An efficient convex formulation for model-predictive control on wave-energy converters," *Journal of Offshore Mechanics and Arctic Engineering*, vol. 140, no. 3, 2018.

[30] F. Allgöwer and A. Zheng, *Nonlinear model predictive control*. Birkhäuser, 2012, vol. 26.

[31] G. Li, "Nonlinear model predictive control of a wave energy converter based on differential flatness parameterisation," *International Journal of Control*, vol. 90, no. 1, pp. 68–77, 2017.

[32] J. Na, B. Wang, G. Li, S. Zhan, and W. He, "Nonlinear constrained optimal control of wave energy converters with adaptive dynamic programming," *IEEE Transactions on Industrial Electronics*, vol. 66, no. 10, pp. 7904–7915, 2018.

[33] A. S. Haider, T. K. Brekken, and A. McCall, "Real-time nonlinear model predictive controller for multiple degrees of freedom wave energy converters with non-ideal power take-off," *Journal of Marine Science and Engineering*, vol. 9, no. 8, p. 890, 2021.

[34] M. Previsic, A. Karthikeyan, and D. Lyzenga, "In-ocean validation of a deterministic sea wave prediction (dswp) system leveraging x-band radar to enable optimal control in wave energy conversion systems," *Applied Ocean Research*, vol. 114, p. 102784, 2021.

[35] O. Abdelkhalik, S. Zou, R. Robinett, G. Bacelli, and D. Wilson, "Estimation of excitation forces for wave energy converters control using pressure measurements," *International Journal of Control*, vol. 90, no. 8, pp. 1793–1805, 2017.

[36] F. Fusco and J. V. Ringwood, "Short-term wave forecasting for real-time control of wave energy converters," *IEEE Transactions on sustainable energy*, vol. 1, no. 2, pp. 99–106, 2010.

[37] M. P. Schoen, J. Hals, and T. Moan, "Wave prediction and robust control of heaving wave energy devices for irregular waves," *IEEE Transactions on energy conversion*, vol. 26, no. 2, pp. 627–638, 2011.

[38] G. Li, G. Weiss, M. Mueller, S. Townley, and M. R. Belmont, "Wave energy converter control by wave prediction and dynamic programming," *Renewable Energy*, vol. 48, pp. 392–403, 2012.

[39] U. A. Korde, "Near-optimal control of a wave energy device in irregular waves with deterministic-model driven incident wave prediction," *Applied Ocean Research*, vol. 53, pp. 31–45, 2015.

[40] A. F. Davis and B. C. Fabien, "Wave excitation force estimation of wave energy floats using extended kalman filters," *Ocean Engineering*, vol. 198, p. 106970, 2020.

[41] S. Mavrakos and P. McIver, "Comparison of methods for computing hydrodynamic characteristics of arrays of wave power devices," *Applied Ocean Research*, vol. 19, no. 5-6, pp. 283–291, 1997.

[42] M. Folley, A. Babarit, B. Child, D. Forehand, L. O?Boyle, K. Silverthorne, J. Spinneken, V. Stratigaki, and P. Troch, "A review of numerical modelling of wave energy converter arrays," in *International Conference on Offshore Mechanics and Arctic Engineering*, vol. 44946. American Society of Mechanical Engineers, 2012, pp. 535–545.

[43] S. J. Beatty, M. Hall, B. J. Buckham, P. Wild, and B. Bocking, "Experimental and numerical comparisons of self-reacting point absorber wave energy converters in regular waves," *Ocean Engineering*, vol. 104, pp. 370–386, 2015.

[44] B. A. Ling, B. Bosma, and T. K. Brekken, "Experimental validation of model predictive control applied to the azura wave energy converter," *IEEE Transactions on Sustainable Energy*, vol. 11, no. 4, pp. 2284–2293, 2019.

[45] D. Garca-Violini, Y. Pea-Sanchez, N. Faedo, C. Windt, F. Ferri, and J. V. Ringwood, "Experimental implementation and validation of a broadband lti energy-maximizing control strategy for the wavestar device," *IEEE Transactions on Control Systems Technology*, vol. 29, no. 6, pp. 2609–2621, 2021.

[46] Z. Lin, X. Huang, and X. Xiao, "Fast model predictive control system for wave energy converters with wave tank tests," *IEEE Transactions on Industrial Electronics*, 2022.

[47] N. Faedo, Y. Peña-Sanchez, D. Garcia-Violini, F. Ferri, G. Mattiazzo, and J. V. Ringwood, "Experimental assessment and validation of energy-maximising moment-based optimal control for a prototype wave energy converter," *Control Engineering Practice*, vol. 133, p. 105454, 2023.

[48] H. Gu, P. Stansby, T. Stallard, and E. C. Moreno, "Drag, added mass and radiation damping of oscillating vertical cylindrical bodies in heave and surge in still water," *Journal of Fluids and Structures*, vol. 82, pp. 343–356, 2018.

[49] M. Penalba, A. Mérigaud, J.-C. Gilloteaux, and J. V. Ringwood, "Influence of nonlinear froude?krylov forces on the performance of two wave energy points absorbers," *Journal of Ocean Engineering and Marine Energy*, vol. 3, pp. 209–220, 2017.

[50] H. Akçay and S. Türkay, "Power spectrum estimation in innovation models," *Mechanical Systems and Signal Processing*, vol. 121, pp. 227–245, 2019.

[51] Y. Lao, J. T. Scruggs, A. Karthikeyan, and M. Previsic, "Discrete-time causal control of a wave energy converter with finite stroke in stochastic waves," *IEEE Transactions on Control Systems Technology*, vol. 30, no. 3, pp. 1198–1214, 2022.

[52] A. H. Sayed and T. Kailath, "A survey of spectral factorization methods," *Numerical Linear Algebra with Applications*, vol. 8, no. 6-7, pp. 467–496, 2001.

[53] J. A. Cretel, G. Lightbody, G. P. Thomas, and A. W. Lewis, "Maximisation of energy capture by a wave-energy point absorber using model predictive control," *IFAC Proceedings Volumes*, vol. 44, no. 1, pp. 3714–3721, 2011.

[54] B. Anderson and J. Moore, *Optimal Filtering*, ser. Dover Books on Electrical Engineering. Dover Publications, 2012. [Online]. Available: https://books.google.com/books?id=iYMqLQp49UMC

[55] J. Hoagg, S. Lacy, R. Erwin, and D. Bernstein, "First-order-hold sampling of positive real systems and subspace identification of positive real models," in *Proceedings of the 2004 American Control Conference*, vol. 1, 2004, pp. 861–866 vol.1.

[56] Y. Lao and J. T. Scruggs, "A modified technique for spectral factorization of infinite-dimensional systems using subspace techniques," in *2019 IEEE 58th Conference on Decision and Control (CDC)*, 2019, pp. 5412–5419.

[57] A. Mesbah, "Stochastic model predictive control: An overview and perspectives for future research," *IEEE Control Systems Magazine*, vol. 36, no. 6, pp. 30–44, 2016.

[58] O. Faltinsen, *Sea loads on ships and offshore structures*. Cambridge university press, 1993, vol. 1.

[59] M. Grant and S. Boyd, "CVX: Matlab software for disciplined convex programming, version 2.1," http://cvxr.com/cvx, Mar. 2014.

[60] B. Brogliato, R. Lozano, B. Maschke, and O. Egeland, *Dissipative Systems Analysis and Control: Theory and Applications*. Springer, 2019.

Connor Ligeikis (S'21) received the B.S.E. and M.S. degrees in civil engineering from the University of Connecticut, Storrs, CT, USA in 2017 and 2019, respectively. He received the M.S. degree in electrical and computer engineering and the Ph.D. degree in civil engineering from the University of Michigan, Ann Arbor, MI, USA in 2021 and 2023, respectively. He is currently an Assistant Professor in the Department of Mechanical Engineering at Lafayette College, Easton, PA, USA. His research interests include vibration, control, mechatronics, and cyber-physical systems. He was the recipient of a 2019 National Science Foundation Graduate Research Fellowship.

Jeff Scruggs (M'11) is an Associate Professor in the Departments of Civil and Environmental Engineering, as well as of Electrical and Computer Engineering (by courtesy), at the University of Michigan, which he joined in 2011. He received his B.S. and M.S. degrees in Electrical Engineering from Virginia Tech in 1997 and 1999, respectively, and his Ph.D. in Applied Mechanics from the Caltech in 2004. Prior to joining the University of Michigan, he held post-doctoral positions at Caltech and the University of California, San Diego, and was on the faculty at Duke University from 2007-11. Scruggs's current research is in the areas of mechanics, vibration, energy, and control.